



ESA Climate Change Initiative – Fire_cci

O1.D1: Basic consistency of fire observations report

Project Name	ECV Fire Disturbance: Fire_cci Phase 2
Contract N°	4000115006/15/I-NB
Issue Date	23 January 2018
Version	1.0
Author	Angelika Heil, Johannes W. Kaiser
Document Ref.	Fire_cci_O1.D1_v1.0.pdf
Document type	Public

To be cited as: Heil A., Kaiser J.W (2018) ESA CCI ECV Fire Disturbance: O1.D1 Basic consistency of fire observations report, version 1.0. Available at: <http://www.esa-fire-cci.org/documents>

	Fire_cci	Ref.:	Fire_cci_O1.D1_v1.0.docx		
	Option 1 WP110 Basic consistency of fire observation report	Issue	1.0	Date	23/01/2018
			Page	2	

Project Partners

Prime Contractor/ Scientific Lead & Project Management	UAH – University of Alcala (Spain)
Earth Observation Team	UAH – University of Alcala (Spain)
	EHU – University of the Basque Country (Spain)
	UL – University of Leicester (United Kingdom)
	UCL – University College London (United Kingdom)
	ISA – School of Agriculture, University of Lisbon (Portugal)
System Engineering	BC – Brockmann Consult (Germany)
Climate Research Group	MPIC – Max Planck Institute for Chemistry (Germany)
	IRD - Research Institute for Development (France)
	LSCE - Climate and Environmental Sciences Laboratory (France)
	VUA - Vrije Universiteit Amsterdam (Netherlands)



Distribution

Affiliation	Name	Address	Copies
ESA	Stephen Plummer (ESA)	stephen.plummer@esa.int	electronic copy
Project Team	Emilio Chuvieco (UAH)	emilio.chuvieco@uah.es	electronic copy
	M. Lucrecia Pettinari (UAH)	mlucrecia.pettinari@uah.es	
	Joshua Lizundia (UAH)	joshua.lizundia@uah.es	
	Gonzalo Otón (UAH)	gonzalo.oton@uah.es	
	Mihai Tanase (UAH)	mihai.tanase@uah.es	
	Miguel Ángel Belenguer (UAH)	miguel.belenguer@uah.es	
	Aitor Bastarrika (EHU)	aitor.bastarrika@ehu.es	
	Ekhi Roteta (EHU)	ekhi.roteta@gmail.com	
	Kevin Tansey (UL)	kjt7@leicester.ac.uk	
	Marc Padilla Parellada (UL)	mp489@leicester.ac.uk	
	James Wheeler (UL)	jemw3@leicester.ac.uk	
	Philip Lewis (UCL)	ucfalew@ucl.ac.uk	
	José Gómez Dans (UCL)	j.gomez-dans@ucl.ac.uk	
	James Brennan (UCL)	james.brennan.11@ucl.ac.uk	
	Jose Miguel Pereira (ISA)	jmocpereira@gmail.com	
	Duarte Oom (ISA)	duarte.oom@gmail.com	
	Manuel Campagnolo (ISA)	mlc@isa.ulisboa.pt	
	Thomas Storm (BC)	thomas.storm@brockmann-consult.de	
	Johannes Kaiser (MPIC)	j.kaiser@mpic.de	
	Angelika Heil (MPIC)	a.heil@mpic.de	
Florent Mouillot (IRD)	florent.mouillot@cefe.cnrs.fr		
M. Vanesa Moreno (IRD)	mariavanesa.morenodominguez@cefe...		
Philippe Ciais (LSCE)	philippe.ciais@lsce.ipsl.fr		
Chao Yue (LSCE)	chaoyuejoy@gmail.com		
Pierre Laurent (LSCE)	pierre.laurent@lsce.ipsl.fr		
Guido van der Werf (VUA)	guido.vander.werf@vu.nl		
Ioannis Bistinas (VUA)	i.bistinas@vu.nl		



Summary

In Option 1 of the ESA Fire_cci Phase 2 project (RFQ/3-14286/15/I-NB), datasets of burned area from various satellites, fire radiative power from GFAS, fuel consumption, available fuel load and combustion completeness from GFED, and land cover from the ESA LandCover_cci and MODIS have been collected and converted to a consistent data format with consistent temporal and spatial resolutions. This reports describes the consistent datasets, consistency tests performed on them, and gives recommendations on consistency issues that need to be excluded from the combined analysis.

	Affiliation/Function	Name	Date
Prepared	MPIC MPIC	Angelika Heil Johannes Kaiser	23/01/2018
Reviewed	UAH – Project Manager	Lucrecia Pettinari	24/01/2018
Authorized	UAH - Science Leader	Emilio Chuvieco	24/01/2018
Accepted	ESA - Technical Officer	Stephen Plummer	

This document is not signed. It is provided as an electronic copy.

Document Status Sheet

Issue	Date	Details
1.0	24/01/2018	First Issue

Document Change Record

Issue	Date	Request	Location	Details



Table of Contents

1. Introduction	8
2. Option 1 Data Repository	8
2.1. Methods	8
2.2. File formats.....	9
2.3. MERIS Fire_cci v4.1 burned area	10
2.4. MODIS MCD64 Collection 5.1 burned area (MCD64C5 aka "GFED4")	10
2.5. GFED4s burned area	11
2.6. MODIS MCD64 Collection 6 burned area.....	11
2.7. MODIS MCD45 burned area	11
2.8. CAMS Global Fire Assimilation System (GFAS) Fire Radiative Power and (FRP) fuel consumption time series	11
2.9. GFED4s time series of fuel consumption, available fuel load and combustion completeness.....	12
2.10. MODIS MCD12C1 Collection 5.1 land cover dataset	12
2.11. ESA LandCover_cci land cover dataset	13
2.12. Global fuelbed dataset	15
2.13. GFED4s fuel load estimates from the GFED4s modelling framework.....	15
3. Basic consistency assessment of fire observations	15
3.1. Burned area and FRP datasets	15
3.2. Fuel availability and consumption datasets	17
3.3. Land cover datasets	17
3.4. Influence of observational coverage on fuel consumption estimates	18
3.5. Spurious signals in satellite-derived burned area and FRP observations	19
3.6. Inconsistencies between GFED4(s) burned area and GFED4(s) fuel consumption.....	21
4. Representation of individual fires at the pixel and grid level.....	22
4.1. 2005 Black Tuesday Eyre Peninsula bushfire, SA, Australia	22
4.2. 2005 Pickering Brook bushfire, WA, Australia	28
5. Conclusions and Recommendations for WP130	32
6. References.....	33

List of Tables

Table 1: Burned area time series.	9
Table 2: Fire radiative power (FRP), fuel consumption and combustion completeness time series.	9
Table 3: Static maps of land cover and fuel type and characteristics.....	9
Table 4: GFAS parameters included in this study and their specifications.....	12
Table 5: GFED4s parameters included in this study and their specifications.....	12
Table 6: Global area covered by individual MODIS MCD12C1 Collection 5.1 land cover classes across 2001 to 2012. A two-tailed Mann-Kendall test is performed to assess if there is a significant monotonic trend in the annual time series.	13

	Fire_cci Option 1 WP110 Basic consistency of fire observation report	Ref.:	Fire_cci_O1.D1_v1.0.docx		
		Issue	1.0	Date	23/01/2018
				Page	5

Table 7: Global area covered by individual ESA LandCover_cci v2.0.7 land cover classes across 2005 to 2011.	14
Table 8: Aggregation of the ESA LandCover_cci v2.0.7 land cover classes and the MODIS MCD12C1 UMD land cover classes to major land cover categories. (1) is adapted from Table 3-3 in the ESA Land Cover CCI Product User Guide Version 2.0; available online at http://maps.elie.ucl.ac.be/CCI/viewer/download/ESACCI-LC-Ph2-PUGv2_2.0.pdf	18
Table 9: Share of grid cells with non-zero burned area (or FRE), which coincide with grid cells with known eruptive volcanic activity. In addition, the contribution of burned area (FRE) in grid cells with known eruptive volcanic activity to total burned area (FRE) in Indonesia and in Java is given.	20

List of Figures

Figure 1: Dominant MODIS MCD12C1 Collection 5.1 vegetated land cover in 2005 at 0.25 degree resolution. A definition of the land cover classes is given in Table 6. 13	
Figure 2: Dominant ESA LandCover_cciv2.0.7 vegetated land cover in 2005 at 0.25 degree resolution. The codes refer to the codes defined in Table 7.	14
Figure 3: Total available fuel load (in kg C per m ²) derived from the Global fuelbed dataset (Pettinari and Chuvieco 2016).	15
Figure 4: Best estimate ("median") total available fuel load (in kg C per m ²) derived with the GFED4s framework for Fire_cci Option 1 WP120. Total available fuel load is the sum of the median available fuel load estimates for the pools foliage, wood, litter, cwd (coarse litter) and soil.	15
Figure 5: Mean annual burned area proportion (2005-2011) per 0.25 degree grid cell [% year ⁻¹]. In the panels, the mean annual global burned area is given.	16
Figure 6: Mean annual GFAS v1.2 fire radiative energy (FRE) (2005-2011) per 0.5 degree grid cell [log ₁₀ J m ⁻² year ⁻¹].	17
Figure 7: (a) Absolute difference in total available fuel load (in kg C per m ²): Global fuelbed estimate minus GFED4s-derived median estimate (Figure 3 and Figure 4). Only grid cells with non-zero values in both products are shown (left) and (b) relative difference of (a) with respect to the GFED4s-derived estimate (right). When multiplied by the grid area, estimated global available fuel carbon is 242 Pg C in the global fuelbed database, and 186 Pg C in the GFED4s-derived estimate. 17	
Figure 8: Dominant vegetated land cover categories in 2005 in the ESA LandCover_cciv2.0.7 land cover map (left) and the MCD12C1 Collection 051 land cover map (right) in 0.25 degree resolution. The codes refer to the major and cover category codes defined in Table 7.	18
Figure 9: (a) Estimated fuel consumption across 2005 to 2011 (in kg C per m ² burned) derived from the ratio of the time-integrals of GFAS carbon emissions and Fire_cci v4.1 total area burned. The calculation is performed with 0.5 degree spatially gridded products (left). (b) Same as (a), but masking for incomplete observations is applied prior the ratio calculation. It means that when observational coverage in Fire_cci v4.1 is incomplete in a certain month and grid cell, GFAS carbon emissions and Fire_cci burned area are excluded from the calculation.	19
Figure 10: Area burned and FRP across 2006 to 2008 in Austria as mapped by different fire satellite products. Also shown are a map and summary statistics with ground-truthed fires from the Austrian BOKU fire database available online at http://fire.boku.ac.at/public/	20
Figure 11: MCD64C6 monthly burned area in north-eastern Europe in March 2009 (top left) and monthly mean MODIS Collection 6 MOD10CM snow cover fraction (top	



right). The figure at the bottom shows where burned area is mapped on fully snow covered areas. 21

Figure 12: Total of number per months over 2005 to 2011 where GFED4s burned area in GFED4s (left) and GFED4 (right) is greater than zero while the corresponding GFED4s fuel consumption estimate is zero. In total, 52 (left) and 27 (right) grid cells are affected. For the sake of presentability, the figure shows the dataset regridded to 4 degree. 21

Figure 13: Google Earth Map of Eyre Peninsula, South Australia displaying an MODIS Aqua false-colour infrared image that shows huge fires and smoke plumes on January 11, 2005. Places where MODIS detected actively burning fire are outlined in red while areas of intense flaming appear in bright pink. The purple overlay displays the final perimeters of the burn scars as mapped by aircraft on January 17, 2005 (Data source: DEWNR). The bottom right insert illustrates the progression of the fire on January 11th, 2005 by hourly isochrones (Newnham et al. 2013). The red circle shows the approximate area burned on January 10th, 2005 (Johnston et al. 2010). 22

Figure 14: (a) Final perimeter of the burn scar as mapped by aircraft on January 17, 2005 (Data source: DEWNR(4)) for the domain of the Black Tuesday Eyre Peninsula bushfires (LON LAT box: 135.5,136.03,-34.65,-34.34). The actual fire event took place between Day of Burn (DOB) 10 to 12. Total area burned is given in the top left of the panel (left). (b) Map indicating the fuel load distribution. The map is derived by combining the fuel load estimates for different fuel categories by Newnham et al. (2013) with the LandCover_cci land cover map of the year 2004 (right). 24

Figure 15: Day of burn (DOB) as given in pixel products for January to February 2005 for the domain of the Black Tuesday Eyre Peninsula bushfires. In the top left of each panel, the DOB range and the total area burned (BA) is given. The actual fire event took place between DOB 10 to 12. 24

Figure 16: Day of burn (DOB) as given in the Fire_cci MODIS v5.0 pixel products for January to February 2005 for the domain of the Black Tuesday Eyre Peninsula bushfires. 25

Figure 17: (a) Same as Figure 15 top left, but with different scaling (left). (b) Confidence level as given in the Fire_cci 4.1 pixel product for January and February 2005 (right). 25

Figure 18: Density scatter plot relating Fire_cci 4.1 date of burn (DOB) and the corresponding confidence level for the domain of the Black Tuesday Eyre Peninsula bushfires across January and February 2005. The colour indicates the number density. In addition, the median confidence level per DOB is plotted..... 25

Figure 19: Burned area (BA) in South Australia in January 2005 as mapped by different inventories. REF denotes the aerial mapped burn scar reference as given by DEWNR⁽⁴⁾. 26

Figure 20: (a) Biweekly burned area (BA) (left) and (b) number of burn patches (NP) (right) in South Australia in January and February 2005 as mapped by Fire_cci 4.1. 27

Figure 21: (a) Absolute burned area bias (Fire_cci 4.1 minus REF) and Fire_cci 4.1 standard error (SE) for the month January 2005. The SE is calculated from the biweekly standard errors by the root sum of the squares approach (Ratcliffe and Ratcliffe 2015). In the top insert, the 99% confidence intervals (CI) for the gridded Fire_cci burned area estimates for January 2005 and the corresponding reference BA values are shown (left). (b) Biweekly fraction of observed area in South Australia in January and February 2005 as mapped by Fire_cci (right). 27



Figure 22: Same as Figure 21a, but for GFED4. 28

Figure 23: Burn scar (blue outline) of the Pickering Brook wildfire in January 2005 as mapped by aerial multispectral line scanning (Source: https://www.dpaw.wa.gov.au/images/documents/get-involved/n2n/schools/excursions/overlay_map1.jpg). The red lines schematically contour the perimeter of the area burned until January 16th, 10pm local time (Cheney 2010). 29

Figure 24: Day of burn (DOB) as given in pixel products for January to February 2005 for the domain of the Pickering Brook bushfire (LON LAT box: 116.05,116.45,-32.17,-31.96, grid lines with 0.05 degree spacing). In the top left of each panel, the DOB range is and the total area burned is given. The actual fire event took place between DOB 15 to 25. In the MODIS products, there is a separate around 4 km² burn patch at 31.15 deg South and 116.1 deg East with DOB between 43 to 52 which is masked out here..... 30

Figure 25: Density scatter plot relating Fire_cci 4.1 date of burn (DOB) and the corresponding confidence level for the domain of the Pickering Brook wildfire across January and February 2005. The colour indicates the number density. In addition, the median confidence level per DOB is plotted..... 30

Figure 26: Burned area and FRR estimated for January and February 2005 for the Pickering Brook wildfire. Estimates are given for individual 0.25 grid cells and as summary statistics for the entire domain. 31



1. Introduction

Option 1 of the ESA Fire_cci Phase 2 project (RFQ/3-14286/15/I-NB) performs a combined analysis of burned area (BA), fire radiative power (FRP) and related datasets in order to derive information on the fuel consumption per unit area and the FRP-DM conversion factor, which are used in the calculation of the pyrogenic carbon flux in BA- and FRP-based inventories, respectively.

In this work package, datasets of burned area from various satellites, fire radiative power from GFAS, fuel consumption, available fuel load and combustion completeness from GFED, and land cover from the ESA LandCover_cci and MODIS have been collected and converted to a consistent data format with consistent temporal and spatial resolutions.

Chapter 2 of this report describes the converted datasets that have been generated and archived for Option 1. Chapter 3 presents a basic consistency analysis of the different fire observation and fuel characterisation datasets included in the repository. Chapter 4 tests the representation of two large, well-documented fires in the different fire observational datasets. Chapter 5 summarises the conclusions drawn in this report.

2. Option 1 Data Repository

2.1. Methods

A data repository with consistent datasets of satellite-based burned area (BA), fire radiative power (FRP), fire-related fuel consumption estimates and fuel characteristic maps is created. The datasets are standardised in terms of file format and data format and temporal and spatial resolutions. Standardisation allows for immediate inter-comparison of the data.

All datasets in the repository are global, 0.25 degree spatially gridded fields. The repository consists of time series and of global static maps. All time series have a monthly time resolution and cover the period January 2005 to December 2011. "Static" maps consist of single fields and are approximately representative for the entire 2005 to 2011 period. In the case of the MODIS and LandCover_cci land cover maps, they have annual temporal resolution.

Table 1 to Table 3 provide information on the datasets included into the Option 1 data repository.

Most of the burned area and fuel consumption time series (e.g. GFED4(s), gridded Fire_cci product) stored in the Option 1 data repository were already provided in 0.25 degree resolution. For all other products, 0.25 degree gridded burned area information is computed from the product's pixel level. MCD64C5 and MCD64C6, which are provided in sinusoidal projection, are first reprojected with GDAL to WGS84. Burned pixels are identified from the burn date layer contained in the monthly files and the area of all burned pixels falling in the domain of each 0.25 degree grid is computed.

Table 1: Burned area time series.

Product acronym	Fire_cci	MCD64C5	MCD45	GFED4	GFED4s
Burned area product's full name	ESA MERIS Fire_cci v4.1	MCD64A1 MODIS Collection 5.1	MCD45A1 MODIS Collection 5.1	MCD64A1 MODIS Collection 6	Global Fire Emissions Database version 4.1 (GFED4s) with small fires
Original spatial resolution	300 m; 0.25°	500 m	500 m	500 m	0.25°
Temporal coverage	2005-2011	2000-2016	2000-2016	2000-2016	1997-2015
Data availability	https://geogra.uah.es/fire_cci/	ftp://fuoco.geog.udel.edu (folder /db/MCD64A1)	ftp://ba1.geog.udel.edu (folder /Collection51)	ftp://ba1.geog.udel.edu (folder /Collection6)	http://www.globalfiredata.org/data.html

Table 2: Fire radiative power (FRP), fuel consumption and combustion completeness time series.

Product acronym	GFAS	GFED4s
Product's full name	Global Fire Assimilation System v1.2	Global Fire Emissions Database version 4.1 (GFED4s) with small fires
Original spatial resolution	0.1°	0.25°
Temporal coverage	2000-NRT	1997-2015
Data availability	http://www.gmes-atmosphere.eu/oper_info/global_nrt_data_access/gfas_ftp/	http://www.globalfiredata.org/data.html

Table 3: Static maps of land cover and fuel type and characteristics.

Product acronym	Global Fuelbed Dataset	MODIS Land Cover Map	LandCover_cci Land Cover Map
Product's full name	Global Fuelbed Dataset https://doi.org/10.1594/PAN_GAEA.849808	Global MODIS MCD12C1 Collection 051 Land Cover maps	Global CCI Land Cover maps v2.07
Original spatial resolution	300 m	500 m	300 m
Temporal representativity	~2005	Annual maps 2005-2011	Annual maps 2005-2011
Data availability	https://doi.org/10.1594/PAN_GAEA.849808	http://e4ftl01.cr.usgs.gov/MOTA/MCD12C1.051/	ftp://anonymous:fireftp%40example.com@geo10.elie.ucl.ac.be/v207/

2.2. File formats

All Option 1 datasets are provided on the ftp-site as global, 0.25 degree spatially resolved netCDF (Network Common Data Format) files.

The filename nomenclature is as follows:

$\{\text{PROD}\}.\{\text{VAR}\}.\{\text{AVG}\}.\{\text{YYYY}\}.\{\text{GRID}\}.\text{nc}$

	Fire_cci		Ref.:	Fire_cci_O1.D1_v1.0.docx		
	Option 1 WP110 Basic consistency of fire observation report		Issue	1.0	Date	23/01/2018
					Page	10

PROD: Product acronym name, see Table 1 to Table 3

VAR: Variable name

AVG: Time averaging method, e.g. MONMEAN for monthly mean, STATIC for static maps

YYYY: Year to which the data is referring

GRID: $r\{NLON\} \times r\{NLAT\}$; $r1440 \times 720$ (default). It specifies the number of grid cells in longitudinal (NLON) and latitudinal (NLAT) direction. In a global regular (r) grid, NLON=1440 and NLAT refers to 0.25 degree spatial resolution. The first grid cell centre in longitudinal direction is set to -179.875 degree, the first grid cell centre in latitudinal direction is set to -89.875.

2.3. MERIS Fire_cci v4.1 burned area


The MERIS Fire_cci v4.1 burned area product has been generated by the ESA Fire_cci project using a burned area detection algorithm that combines temporal changes in near infrared (NIR) MERIS corrected reflectances with active fire detections from the MODIS thermal anomalies product, following a two-phase algorithm (Alonso-Canas and Chuvieco, 2015). Fire_cci v4.1 is comprised of a pixel burned area product (spatial resolution of approx. 300m) with date of detection, burn detection confidence level and land cover information. It also includes a biweekly grid product at 0.25 degree spatial resolution with auxiliary layers comprising standard error, fraction of observed area, number of burn patches and land cover type burned (Pettinari et al. 2016).

2.4. MODIS MCD64 Collection 5.1 burned area (MCD64C5 aka "GFED4")

The MODIS Collection 5.1 burned area product maps post-fire burned areas using daily 500-m MODIS imagery coupled with 1-km MODIS active fire observations. The automated hybrid algorithm applies dynamic thresholds to composite imagery generated from a burn-sensitive vegetation index derived from two short-wave infrared MODIS channels and an index quantifying the change in temporal texture following a potential burn. Cumulative active fire maps are used to guide the selection of burned and unburned training samples and to guide the specification of prior probabilities (Giglio et al., 2009). The official MODIS short name of the product is MCD64A1. In this document, we use the abbreviation MCD64C5.

MCD65C5 is distributed as monthly HDF tiles in sinusoidal projection. The product contains five data layers. One layer specifies the ordinal day of burn (1-366) for each 500-m pixel burn and flags unburned land pixels with 0 and unmapped pixels due to insufficient data or water with -1. The other layers provide information on quality assurance and on the duration of the burn signal and the uncertainty in the date of burn. The latter also contains the water mask required to separate unmapped pixels into missing observations and water pixels.

In the MODIS era (from August 2000 to present), 0.25 degree spatially aggregated MCD64C5 burned area information comprises the burned area component of the Global Fire Emission Database version 4 (GFED4), described in Giglio et al. (2013). In addition to the estimated area burned, the GFED4 burned area product provides ancillary information on the uncertainty and on the type of vegetation burned. Please note that the differences between the GFED4 product compiled by Giglio et al. (2013)

	Fire_cci Option 1 WP110 Basic consistency of fire observation report	Ref.:	Fire_cci_O1.D1_v1.0.docx			
		Issue	1.0	Date	23/01/2018	
				Page	11	

and the gridded MCD64C5 product generated here are within 0.1% when annual global totals across 2005 to 2011 are compared.

2.5. GFED4s burned area

GFED4s is the latest GFED version and was released in May 2015. The burned area component of GFED4s consists of (1) the GFED4 burned area database (see Section 2.4) and (2) a complementary experimental estimate for burned area by "small" fires using an update of the Randerson et al. (2012) approach. GFED4s is described in van der Werf et al. (2017). The experimental small fire database estimates the burned area from small fires, which fall below the detection limit of the MODIS MCD64 Collection 5.1 burned area product. Burned area from these fires is estimated from active fire counts, which are detected outside of the observed MODIS burned area perimeters. For scaling fire counts to burned area, Randerson et al. (2012) use the ratio of burned area to active fires calculated from observations within MODIS burned area perimeters stratified by vegetation types, continental-scale regions, seasonal periods, and years.

GFED4s is provided as hdf5 containing various data layers. The burned area component of GFED4s comprises a burned fraction and a data source layer.

2.6. MODIS MCD64 Collection 6 burned area

The Collection 6 MODIS burned area product, MCD64A1 Collection 6 - here abbreviated with MCD64C6 - was released in January 2017. The product has several improvements with respect to MCD64C5 described in Section 2.4. First of all, MCD64C6 uses MODIS Collection 6 surface reflectances and active fire data as input instead of those from Collection 5.1 in MCD64C5. Secondly, algorithmic improvements were implemented. Together, this leads to reduction of (a) omission errors, in particular those related to the small fires, (b) burn-date temporal uncertainty and (c) the number of unclassified grid cells. In addition, spatial product coverage was expanded and a unique flag for water and for missing data was introduced in the burn date layer (Giglio et al., 2016). Just as the MCD64C5 product, the MCD64C6 is provided as monthly HDF with similar data structure and format.

2.7. MODIS MCD45 burned area

The MCD45 burned area mapping approach is based on a prognostic model of estimated versus actual reflectance for different MODIS spectral bands (Roy et al. 2005) and does not rely on active fire information to identify pixels more likely to be burned. The GeoTiff version of the monthly MCD45 product has a temporal filtering (Roy et al., 2008) applied to exclude any overlap between consecutive months. The data layers define for each pixel the approximate Julian day of burning or a code indicating unburned, no burning detected but snow detected, no burning detected but water detected, or insufficient number of observations to make a detection decision (usually due to cloud or missing data). MCD64C6 supersedes the MCD45 burned area product and MCD45 production has been discontinued in January 2017.

2.8. CAMS Global Fire Assimilation System (GFAS) Fire Radiative Power and (FRP) fuel consumption time series

The Copernicus Atmosphere Monitoring Service (CAMS) has been developed to provide accurate monitoring and daily forecasting of atmospheric composition and air

quality. The CAMS atmospheric models require global estimates on fire emission input fields, which are provided in near-realtime by the Global Fire Assimilation System (GFAS). GFAS is based on satellite-based observations of Fire Radiative Power (FRP) and is described in detail in Kaiser et al. (2012). The most current publically available GFAS version is version 1.2. It provides assimilated daily FRP observations derived from the MODIS Collection 5 product. It also provides derived estimates of biomass burning fuel consumption and emissions at 0.1 degree spatial resolution. GFAS fire and emission estimates are available for the period from 2000 to now via http://gmes-atmosphere.eu/about/project_structure/input_data/d_fire/.

Table 4 shows the GFAS variables included into the Fire_cci Option 1 data repository.

Please note that a new GFAS version relying on the MODIS Collection 6 active fire product is currently being completed. This version has 0.05 degree spatial resolution and 0.25 degree aggregated data from this version will be included into the Option 1 repository as soon as available.

Table 4: GFAS parameters included in this study and their specifications.

Variable	Name ⁽¹⁾	Short name ⁽¹⁾ /paramId ⁽²⁾	Units ⁽¹⁾
FRP	Wildfire radiative power	frpfire (210099)	W m-2
DM	Wildfire combustion rate	crfire (210100)	kg m-2 s-1
C	Wildfire overall flux of burned carbon	cfire (210092)	kg m-2 s-1

⁽¹⁾As defined in <http://apps.ecmwf.int/codes/grib/param-db>. ⁽²⁾paramId refers to the GRIB parameter code.

2.9. GFED4s time series of fuel consumption, available fuel load and combustion completeness

GFED4s described in Section 2.5 estimates global fire carbon (C) and dry matter (DM) emissions, and the contribution of different fire types to these emissions in order to calculate trace gas and aerosol emissions using emission factors. Fire type-specific fuel loads and combustion completeness required for these estimates were derived by combining burned area data with a revised version of the biogeochemical model, Carnegie-Ames-Stanford Approach (CASA-GFED).

Table 5: GFED4s parameters included in this study and their specifications.

Variable	Name	Units
DM	Fuel consumption in mass dry matter (DM) burned	kg m-2
C	Fire-related carbon emissions	kg C m-2
AFL	Aboveground fuel load (AFL) based on GFED and Fire CCI MERIS data	kg C m-2
CC	Combustion completeness (CC) based on GFED and Fire CCI MERIS data	unitless

2.10. MODIS MCD12C1 Collection 5.1 land cover dataset

Annual global, 0.25 degree gridded maps showing the dominant vegetated land cover type were created from the MODIS MCD12C1 Collection 5.1 product using the UMD classification. Global summary statistics by land cover class and an example global map is given in Table 6 and Figure 1.

Table 6: Global area covered by individual MODIS MCD12C1 Collection 5.1 land cover classes across 2001 to 2012. A two-tailed Mann-Kendall test is performed to assess if there is a significant monotonic trend in the annual time series.

Area in mio. km ²		Global total area (area sum over all UMD Codes) is 510.1 mio km ²													Mann-Kendall-Test	p-value
UMD Code	UMD Class	Abbrev.	2001	2002	2003	2004	2005	2006	2007	2008	2009	2010	2011	2012		
0	Water	WAT	366.8	365.6	365.4	365.3	365.3	364.9	365.0	364.8	365.3	365.2	365.3	365.0	decreasing	0.02
1	Evergreen Needleleaf forest	ENF	3.1	2.9	2.7	2.6	2.8	3.1	3.5	3.5	3.2	3.3	3.3	4.0	increasing	0.02
2	Evergreen Broadleaf forest	EBF	12.4	13.4	13.7	13.6	13.5	13.3	13.3	13.5	13.3	13.6	13.7	13.9	no trend	0.14
3	Deciduous Needleleaf forest	DNF	1.4	1.8	1.8	1.9	1.5	1.6	1.5	1.5	1.5	1.5	1.6	1.6	no trend	0.83
4	Deciduous Broadleaf forest	DBF	2.0	1.7	1.8	1.8	1.9	1.8	1.7	1.8	1.8	1.9	1.8	1.8	no trend	1.00
5	Mixed forest	MIF	8.2	8.2	8.1	8.1	8.2	8.5	8.7	8.9	9.2	9.4	9.7	9.9	increasing	0.00
6	Closed shrublands	CSH	0.6	0.4	0.4	0.3	0.3	0.3	0.3	0.3	0.3	0.3	0.4	0.2	decreasing	0.04
7	Open shrublands	OSH	19.9	20.2	20.7	20.9	20.7	21.1	20.7	21.2	21.0	20.9	20.7	20.4	no trend	0.33
8	Woody savannas	WSA	13.0	13.0	12.6	12.8	12.7	12.4	12.3	12.0	12.1	12.3	12.2	12.2	decreasing	0.00
9	Savannas	SAV	11.7	11.6	11.3	10.8	11.4	11.5	11.7	11.7	11.6	10.9	10.7	10.3	no trend	0.15
10	Grasslands	GRA	19.5	19.7	20.0	20.3	20.2	20.0	19.9	19.4	19.4	19.5	20.2	19.6	no trend	0.63
12	Croplands	CRO	15.8	16.0	16.3	16.6	16.5	16.4	16.3	16.2	16.5	16.2	15.9	16.2	no trend	0.78
13	Urban and built-up	URB	0.6	0.6	0.6	0.6	0.6	0.6	0.6	0.6	0.6	0.6	0.6	0.6	no trend	1.00
16	Barren or sparsely vegetated	BSV	35.2	35.2	34.7	34.4	34.2	34.4	34.4	34.6	34.3	34.5	34.0	34.2	decreasing	0.02
Global total vegetated area (Codes 1 to 12)			107.4	108.7	109.2	109.8	109.9	110.1	110.0	110.0	109.9	109.8	110.1	110.2	increasing	0.00

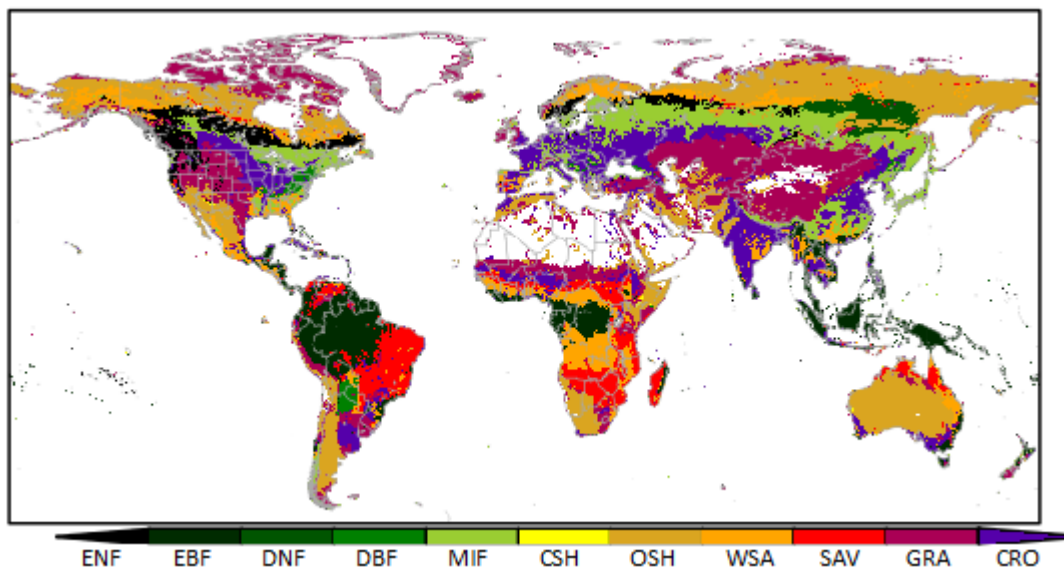


Figure 1: Dominant MODIS MCD12C1 Collection 5.1 vegetated land cover in 2005 at 0.25 degree resolution. A definition of the land cover classes is given in Table 6.

2.11. ESA LandCover_cci land cover dataset

Annual global, 0.25 degree gridded maps showing the dominant vegetated land cover type were created from the ESA LandCover_cci version 2.0.7 land cover product using the LCCS classification. Global summary statistics by land cover class and an example global map is given in Table 7 and Figure 2.

Table 7: Global area covered by individual ESA LandCover_cci v2.0.7 land cover classes across 2005 to 2011.

LCCS Code	LCCS Class	Area in mio. km ²						
		Year						
		2005	2006	2007	2008	2009	2010	2011
10,11,12	Rainfed cropland	15.9	15.9	15.9	16.0	16.0	16.0	16.0
20	Irrigated cropland	2.4	2.4	2.4	2.4	2.4	2.4	2.4
30	Mosaic cropland (>50%)/ natural vegetation (tree, shrub,herbaceous cover) (<50%)	3.9	3.9	3.9	3.9	3.9	3.9	3.9
40	Mosaic natural vegetation (tree, shrub, herbaceous cover) (>50%)/ cropland (< 50%)	3.6	3.6	3.6	3.6	3.6	3.6	3.6
50	Tree cover, broadleaved, evergreen, closed to open (>15%)	12.8	12.8	12.8	12.8	12.8	12.8	12.8
60,61,62	Tree cover, broadleaved, deciduous, closed to open (> 15%)	10.4	10.4	10.4	10.4	10.4	10.4	10.4
70,71,72	Tree cover, needleleaved, evergreen, closed to open (> 15%)	9.0	9.0	9.0	8.9	8.9	8.9	8.9
80,81,82	Tree cover, needleleaved, deciduous, closed to open (> 15%)	5.1	5.1	5.1	5.1	5.1	5.1	5.1
90	Tree cover, mixed leaf type (broadleaved and needleleaved)	2.2	2.2	2.2	2.2	2.2	2.2	2.2
100	Mosaic tree and shrub (>50%) / herbaceous cover (< 50%)	3.3	3.3	3.3	3.4	3.4	3.4	3.4
160	Tree cover, flooded, fresh or brakish water	0.9	0.9	0.9	0.9	0.9	0.9	0.9
170	Tree cover, flooded, saline water	0.2	0.2	0.2	0.2	0.2	0.2	0.2
110	Mosaic herbaceous cover (>50%) / tree and shrub (<50%)	1.1	1.1	1.1	1.1	1.1	1.1	1.1
130	Grassland	12.6	12.6	12.6	12.6	12.6	12.6	12.7
180	Shrub or herbaceous cover, flooded, fresh-saline or brakish water	1.9	1.9	1.9	1.9	1.9	1.9	1.9
190	Urban	0.6	0.6	0.6	0.6	0.6	0.6	0.7
120,121,122	Shrubland	13.3	13.3	13.3	13.3	13.3	13.3	13.3
140	Lichens and mosses	1.5	1.5	1.5	1.5	1.5	1.5	1.5
150,151,152,153	Sparse vegetation (tree, shrub, herbaceous cover)	8.9	8.9	8.9	8.9	8.9	8.9	8.9
200,201,202	Bare areas	19.5	19.5	19.5	19.4	19.4	19.4	19.4
210	Water	366.3	366.3	366.3	366.3	366.3	366.3	366.3
220	Permanent snow and ice	14.6	14.6	14.6	14.6	14.6	14.6	14.6
Global total vegetated area (LCCS Codes 10 to 180)		100.2	100.2	100.2	100.2	100.2	100.2	100.2

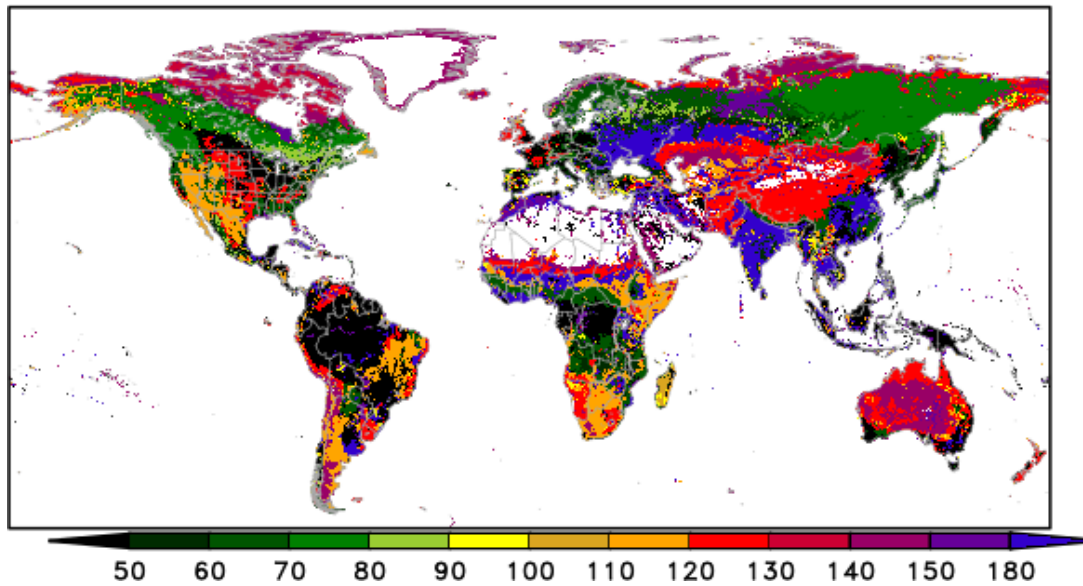


Figure 2: Dominant ESA LandCover_cciv2.0.7 vegetated land cover in 2005 at 0.25 degree resolution. The codes refer to the codes defined in Table 7.

2.12. Global fuelbed dataset

The original global fuelbed dataset of Pettinari & Chuvieco (2016) is provided in 300 m spatial resolution. To obtain a 0.25 degree product, the original information was aggregated to 0.05 degree resolution.

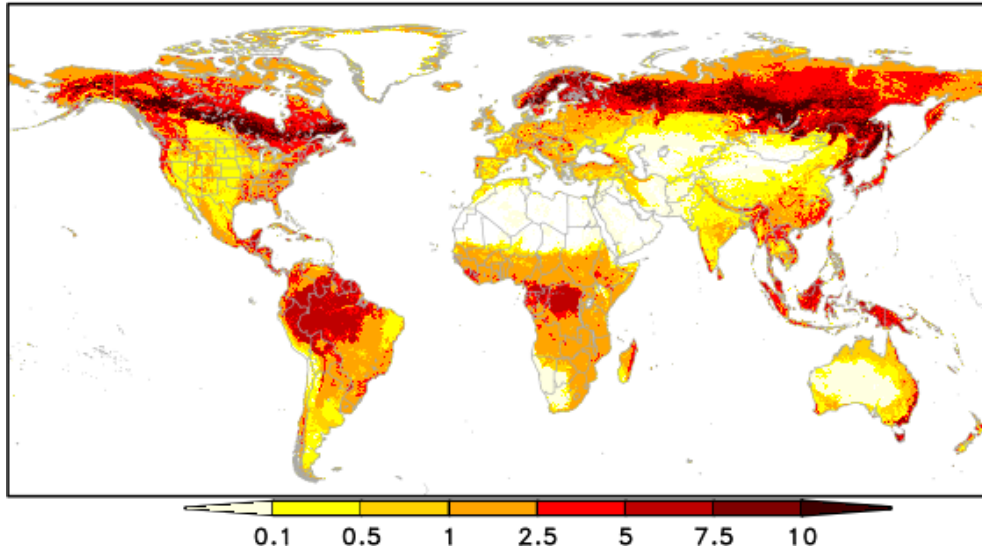


Figure 3: Total available fuel load (in kg C per m²) derived from the Global fuelbed dataset (Pettinari and Chuvieco 2016).

2.13. GFED4s fuel load estimates from the GFED4s modelling framework

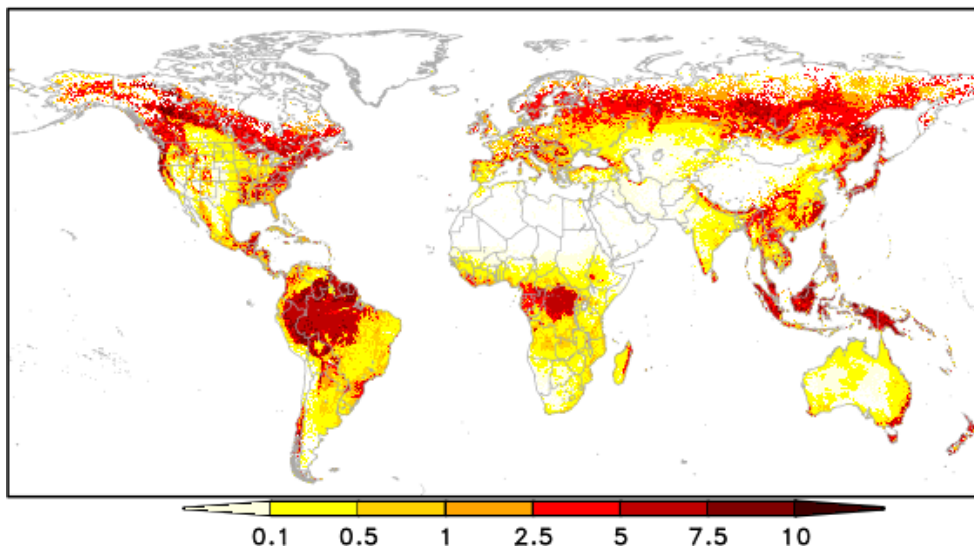


Figure 4: Best estimate ("median") total available fuel load (in kg C per m²) derived with the GFED4s framework for Fire_cci Option 1 WP120. Total available fuel load is the sum of the median available fuel load estimates for the pools foliage, wood, litter, cwd (coarse litter) and soil.

3. Basic consistency assessment of fire observations

3.1. Burned area and FRP datasets

Figure 5 shows the general spatial pattern of mean annual global burned area of all burned area products included in the Fire_cci Option 1 data repository. The figure reflects that all products (i.e. Fire_cci 4.1, MCD64C5, GFED4s, MCD64C6 and

MCD45) largely agree in localizing the regions with most intense fire activity in the tropical belts of Africa and Australia. Fire_cci 4.1 and MCD64C5 also largely agree in the spatial extent and distribution of regions with relatively low burning rates (mean annual burned area proportion less than ~10%). In comparison, these regions are substantially more widespread in MCD64C6 and MCD45, and notably in GFED4s. Fire_cci 4.1 and MCD64C5 shows fire activity in 34% and 37%, respectively, of all land grid cells (in total 253,674, excluding Greenland and Antarctica). The spatial extent increases to 43% in MCD64C6 and MCD45, and 53% in GFED4s.

Figure 6 shows spatial pattern of mean annually integrated fire radiative power, i.e. the annual fire radiative energy (FRE), as calculated from the GFAS v1.2 product for 2005 to 2011. GFAS FRE agrees with the burned area products shown in Figure 5 in localizing the regions with most intense fire activity, but generally shows much more widespread fire activity across the globe. The figures, however, are not fully comparable because GFAS is shown at 0.5 degree spatial resolution while the burned area products are presented at 0.25 degree spatial resolution.

For the Fire_cci Option 1 fuel consumption constraint analysis, a new GFAS version will be used. It is currently being produced by the German GFAS-CLIM project with a grid definition that is consistent with the gridded burned area products (i.e. target grid of 0.25 degree). Such a common grid will allow for consistent masking and intersecting of the products, which is required for the on-going detailed scientific analysis.

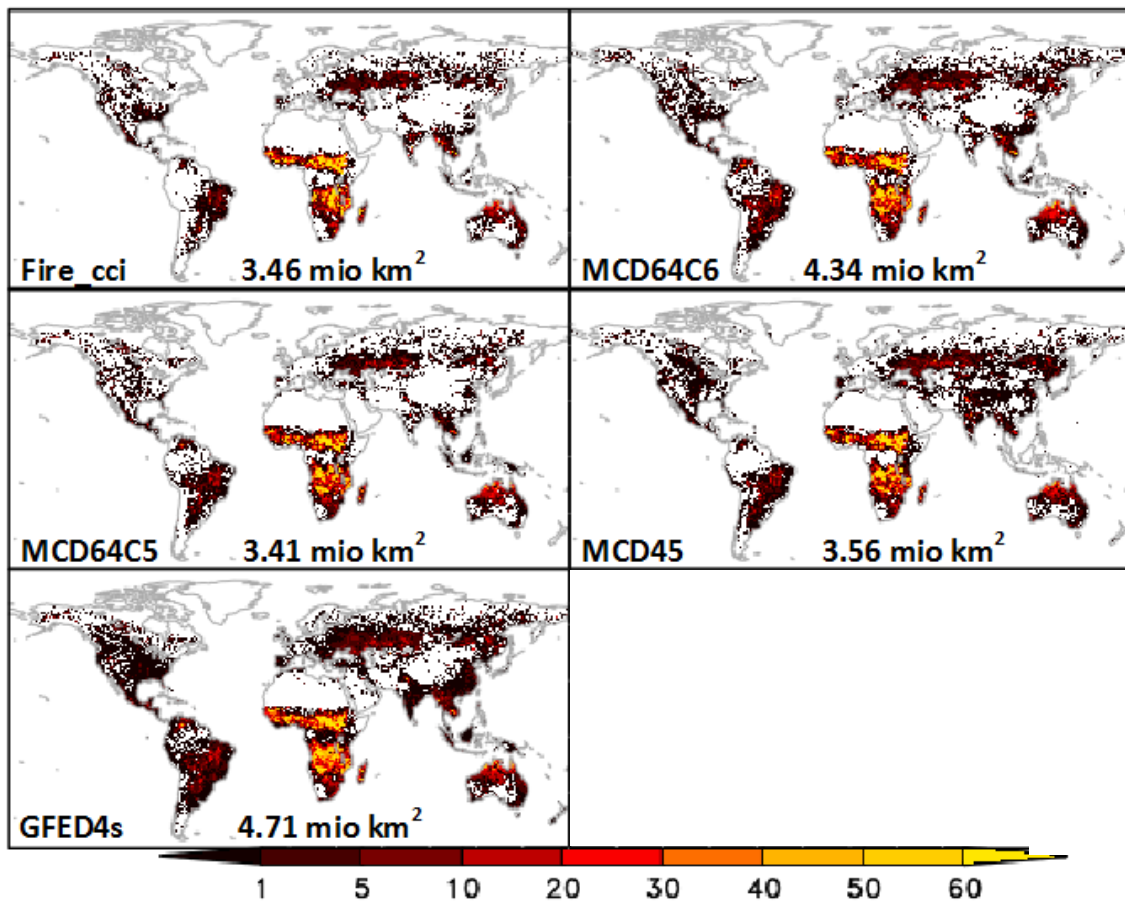


Figure 5: Mean annual burned area proportion (2005-2011) per 0.25 degree grid cell [% year-1]. In the panels, the mean annual global burned area is given.

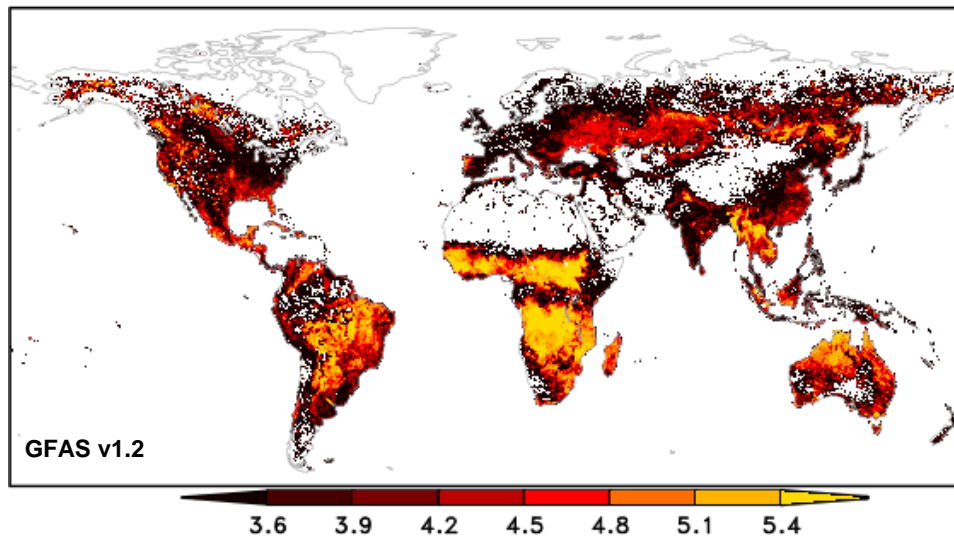


Figure 6: Mean annual GFAS v1.2 fire radiative energy (FRE) (2005-2011) per 0.5 degree grid cell [$\log_{10} \text{ J m}^{-2} \text{ year}^{-1}$].

3.2. Fuel availability and consumption datasets

Figure 7 shows the difference in total available fuel loads between the estimates computed by Pettinari and Chuvieco (2016) with the FCCS global fuelbed approach and by van der Werf (2017) using the GFED4s modelling framework. When comparing only grid cells, which are non-zero in both products, the FCCS approach yields 30% higher global available fuel load estimates than the GFED4s modelling approach. Available fuel loads are higher in particular in the boreal belt and in tropical Africa. In contrast, available fuel load estimates in the FCCS approach are lower tropical and several regions of temperate Europe, conterminous US and Amazonia. The differences reflect the large uncertainties associated with current fuel load estimates, which need to be accounted for in the on-going WP130 analysis.

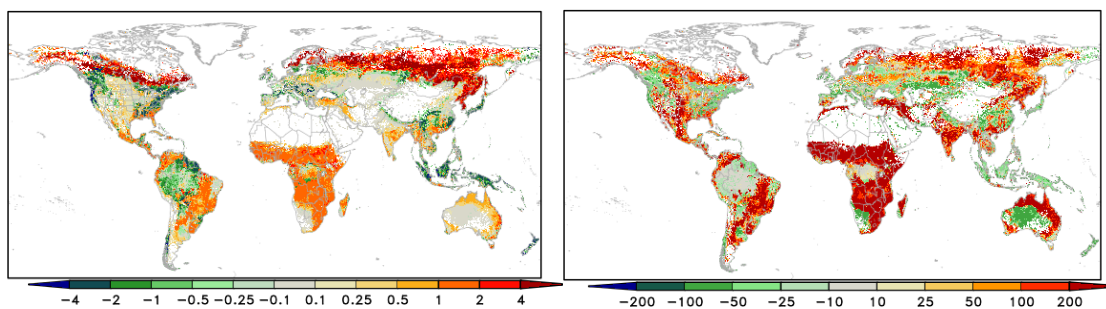


Figure 7: (a) Absolute difference in total available fuel load (in kg C per m²): Global fuelbed estimate minus GFED4s-derived median estimate (Figure 3 and Figure 4). Only grid cells with non-zero values in both products are shown (left) and (b) relative difference of (a) with respect to the GFED4s-derived estimate (right). When multiplied by the grid area, estimated global available fuel carbon is 242 Pg C in the global fuelbed database, and 186 Pg C in the GFED4s-derived estimate.

3.3. Land cover datasets

There is a lot of inconsistency between global land cover datasets because of different input data sources and land cover class definitions used (Bai et al. 2014). Comparison of different land cover maps is therefore limited.

To compare the land cover map of MCD12C1 Collection 051 with the map of ESA LandCover_cciv2.0.7, the individual land cover classes in both products were aggregated to five more generalised common land cover category, namely forest,

agriculture, grassland, shrubland, sparse vegetation. For the two savanna land cover classes contained in the UMD classification (woody savannas and savannas), no common land cover category could be found. Also no common land cover category for the wetland class contained in the LCCS-based ESA LandCover_cci classification system could be worked out. For both, a separate land cover category was established (Table 8). Figure 8 shows a comparison of both land cover maps using this resampling. It illustrates that while the spatial patterns of area classified as agriculture or grassland largely resemble each other, there are strong differences in the areas classified as forest. Due to the different treatment of sparsely vegetated areas, the global vegetated area in MCD12C1 maps, across all years, 10% higher than in the LandCover_cci maps. The difference demonstrates that in any stratification analysis by land cover class, the sensitivity of the results to the choice of the land cover map and the land cover classification system should be carefully examined.

Table 8: Aggregation of the ESA LandCover_cci v2.0.7 land cover classes and the MODIS MCD12C1 UMD land cover classes to major land cover categories. (1) is adapted from Table 3-3 in the ESA Land Cover CCI Product User Guide Version 2.0; available online at http://maps.elie.ucl.ac.be/CCI/viewer/download/ESACCI-LC-Ph2-PUGv2_2.0.pdf.

Major land cover category	vegetated IPCC classes considered for the chance detection ⁽¹⁾	Land_cci land cover map		MODIS MCD12C1 land cover map	
		LCCS Code	LCCS Class	UMD Code	UMD Class
1	Forest	50	Tree cover, broadleaved, evergreen, closed to open (>15%)	2	Evergreen Broadleaf forest
		60,61,62	Tree cover, broadleaved, deciduous, closed to open (> 15%)	4	Deciduous Broadleaf forest
		70,71,72	Tree cover, needleleaved, evergreen, closed to open (> 15%)	1	Evergreen Needleleaf forest
		80,81,82	Tree cover, needleleaved, deciduous, closed to open (> 15%)	3	Deciduous Needleleaf forest
		90	Tree cover, mixed leaf type (broadleaved and needleleaved)		
		100	Mosaic tree and shrub (>50%) / herbaceous cover (< 50%)	5	Mixed forest
		160	Tree cover, flooded, fresh or brackish water		
		170	Tree cover, flooded, saline water		
		10,11,12	Rainfed cropland		
		20	Irrigated cropland		
2	Agriculture	30	Mosaic cropland (>50%) / natural vegetation (tree, shrub, herbaceous cover) (<50%)	12	Croplands
		40	Mosaic natural vegetation (tree, shrub, herbaceous cover) (>50%) / cropland (< 50%)		
		110	Mosaic herbaceous cover (>50%) / tree and shrub (<50%)		
3	Grassland	130	Grassland	10	Grasslands
		120,121,122	Shrubland	7	Open shrublands
4	Other	140	Lichens and mosses	6	Closed shrublands
				150,151,152,153	Sparse vegetation (tree, shrub, herbaceous cover)
5	Sparse vegetation	180	Shrub or herbaceous cover, flooded, fresh-saline or brackish water	n.a.	n.a.
6LCCS	Wetland				
6UMD	Savannas	n.a.	n.a.	8	Woody savannas
				9	Savannas
Global total vegetated area (LCCS Codes 10 to 180)				Global total vegetated area (UMD Codes 1 to	

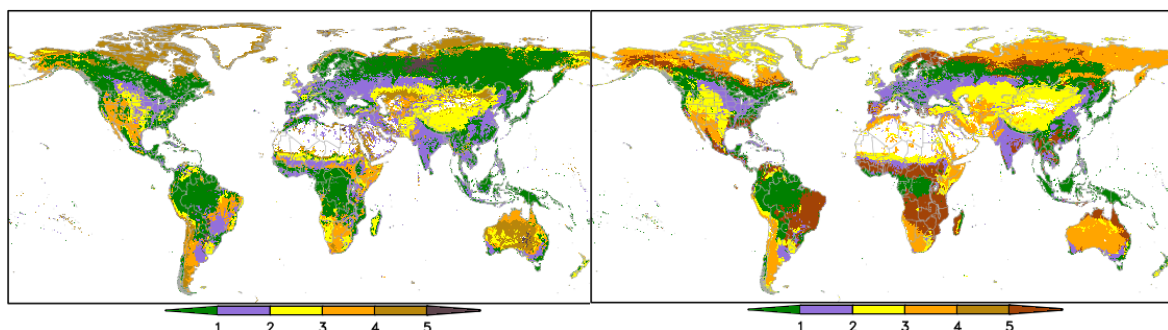


Figure 8: Dominant vegetated land cover categories in 2005 in the ESA LandCover_cci v2.0.7 land cover map (left) and the MCD12C1 Collection 051 land cover map (right) in 0.25 degree resolution. The codes refer to the major and cover category codes defined in Table 7.

3.4. Influence of observational coverage on fuel consumption estimates

One option to constrain fuel consumption is to calculate the ratio between satellite derived fire-related carbon emission estimates (e.g. from GFAS or GFED4s) and

satellite-derived burned area data. Figure 9 illustrates that the derived fuel consumption estimates are highly sensitive to changes in the observational coverage of the burned area observation, using Fire_cci v4.1 as an extreme example since this product is affected by frequent missing observations. Compared to the unmasked approach, the spatial coverage of fuel consumption estimates is lower and over-proportionally restricted to regions with lower fuel consumption estimates. This example highlights the importance of considering the observational coverage in all WP130 analysis.

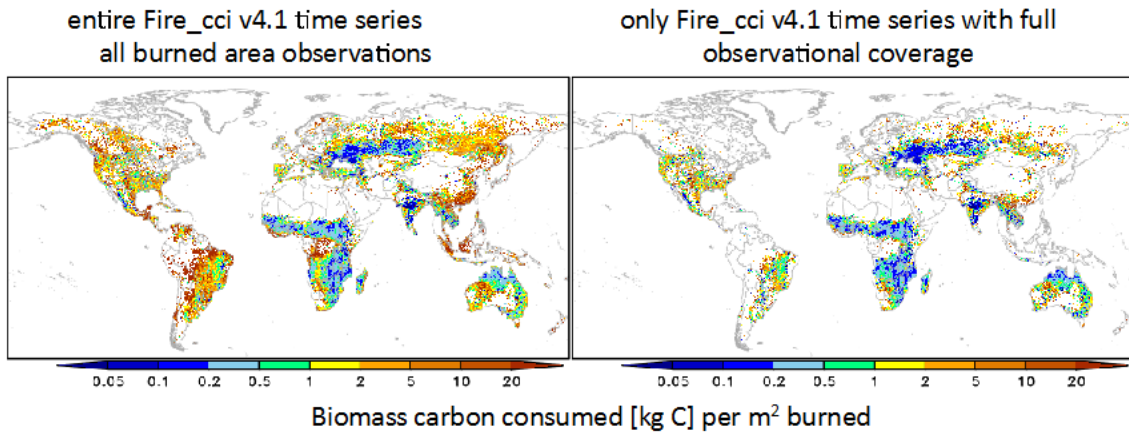


Figure 9: (a) Estimated fuel consumption across 2005 to 2011 (in kg C per m² burned) derived from the ratio of the time-integrals of GFAS carbon emissions and Fire_cci v4.1 total area burned. The calculation is performed with 0.5 degree spatially gridded products (left). (b) Same as (a), but masking for incomplete observations is applied prior the ratio calculation. It means that when observational coverage in Fire_cci v4.1 is incomplete in a certain month and grid cell, GFAS carbon emissions and Fire_cci burned area are excluded from the calculation.

3.5. Spurious signals in satellite-derived burned area and FRP observations

Satellite-derived burned area and FRP observations are subject to various false alarms, which may result in commission errors of regional to global relevance. One cause for non-biomass burning heat signals falsely captured as biomass burning is eruptive volcanic activity. To analyse to what extent spurious volcanic signals contaminate global burned area and FRP products, we extracted the coordinates and exact timing of all eruptive volcanoes across 2005 to 2011 from the "Volcanoes of the World (VOTW)" database of the Smithsonian Institute¹ and aggregated this information to monthly, 0.25 degree gridded mask. Across 2005 to 2011, there are in total 610 eruptive volcanoes. In the different burned area products, 14% (Fire_cci v4.1) to 39% (GFED4s) of the grid cells with volcanic eruptive signals have non-zero burned area. 54% of all eruptive volcanic grid cells show FRP emissions in GFAS (Table 9). In Indonesia, and here particularly on Java island, where there are many active volcanoes, grid cells with volcanic eruptive activity may contribute up to 13% to the total burned area and up to 32% to the total FRP released. This highlights that spurious volcanic signals may strongly influence regional analysis of fuel consumption and it is therefore recommended to carefully mask out spurious signals prior to the Option 1 WP130 analysis.

¹ The database is accessible via http://www.volcano.si.edu/search_eruption.cfm.

Table 9: Share of grid cells with non-zero burned area (or FRE), which coincide with grid cells with known eruptive volcanic activity. In addition, the contribution of burned area (FRE) in grid cells with known eruptive volcanic activity to total burned area (FRE) in Indonesia and in Java is given.

share of eruptive volcanoes that are "burning"			
	global	Indonesia	Java island
Product	% of total number	% of total BA	reprs. FRE
Fire_cci 4.1	14	2.0	13
MCD64C5	18	0.3	9
GFED4s	39	0.5	6
MCD64C6	22	0.2	11
MCD45	19	0.6	4
GFAS v1.3	54	1.5	32

Masking of spurious signals shall also encompass false alarms due to highly reflective surfaces or industrial heat sources. Figure 10 exemplifies for Austria that hybrid burned area products, such as MCD64C5/6 and Fire_cci v4.1, but most notably GFED4s, are affected by false alarms contained in the active fire product, which is used as “seed”. The figure also shows that these false alarms may also affect FRP estimates.

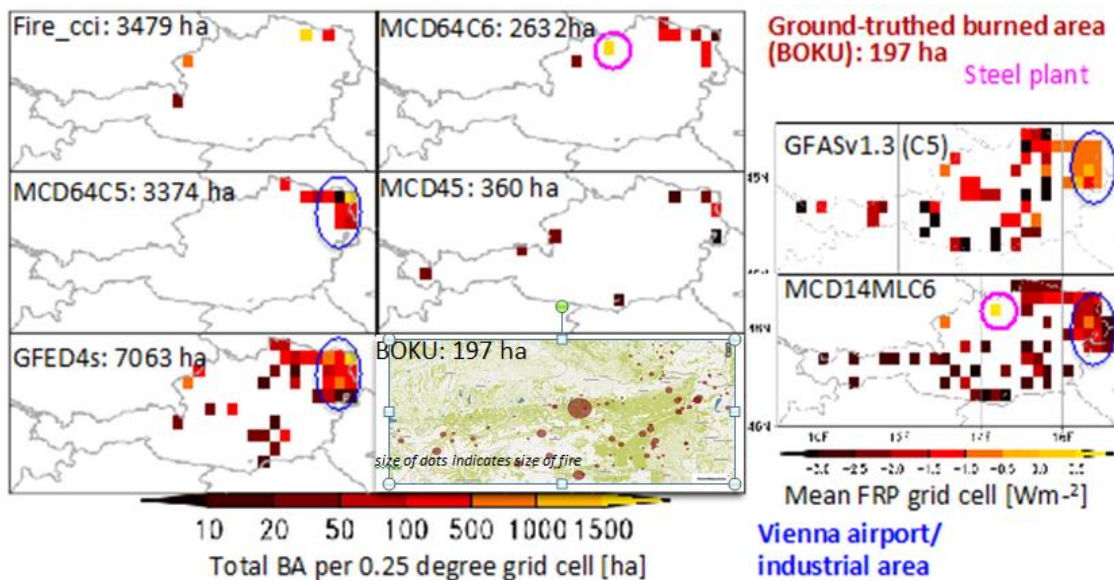


Figure 10: Area burned and FRP across 2006 to 2008 in Austria as mapped by different fire satellite products. Also shown are a map and summary statistics with ground-truthed fires from the Austrian BOKU fire database available online at <http://fire.boku.ac.at/public/>.

Also snow cover, which is a highly reflective surface, could potentially result in spurious fire signals. Figure 11 shows an example where this is likely the case in the MCD64C6 product.

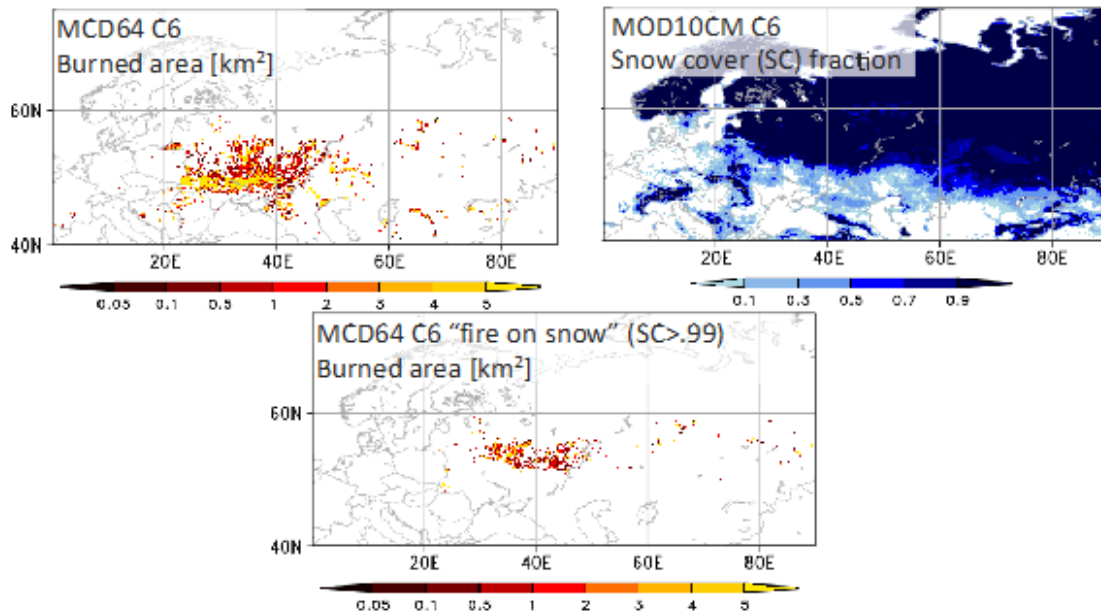


Figure 11: MCD64C6 monthly burned area in north-eastern Europe in March 2009 (top left) and monthly mean MODIS Collection 6 MOD10CM snow cover fraction (top right). The figure at the bottom shows where burned area is mapped on fully snow covered areas.

3.6. Inconsistencies between GFED4(s) burned area and GFED4(s) fuel consumption

Across 2005 to 2011, there are 338 monthly grid cells in GFED4s where there is area burned, but no fuel consumption. In some grid cells, this incongruity occurs repeatedly. The incongruity is less pronounced (in total 62 monthly grid cells) when GFED4s fuel consumption is intersected with the GFED4 burned area data layer instead of the small fire "boosted" GFED4 burned area layer (Figure 12).

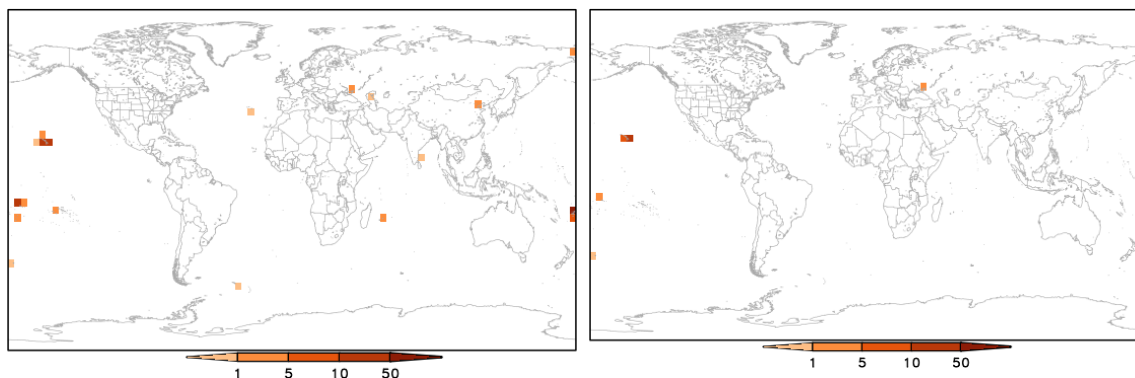


Figure 12: Total of number per months over 2005 to 2011 where GFED4s burned area in GFED4s (left) and GFED4 (right) is greater than zero while the corresponding GFED4s fuel consumption estimate is zero. In total, 52 (left) and 27 (right) grid cells are affected. For the sake of presentability, the figure shows the dataset regridded to 4 degree.

The incongruity primarily affects several remote islands, including Fiji and Hawaii, and is related to the unavailability of satellite information required to calculate net primary

production (NPP) in the GFED-CASA model. As a result, no fuel consumption or emissions are reported for these locations (van der Werf et al., 2017). However, the incongruity does not only occur at land-sea interfaces, but also in the interior of Russia's Far East mainland (not shown). In order to avoid any inconsistencies in the Option 1 analysis, these incongruent grid cells should be masked out. It needs to be explored if the unavailability of satellite information also affects NPP calculation by the GFED-CASA model in other cases as this could further influence the Option 1 analysis.

4. Representation of individual fires at the pixel and grid level

In the following section, we analyse how individual large fires in Australia are represented by different burned area and FRP satellite products in comparison to field-surveyed observations. The results for two large fire events are shown as an example. The analysis focuses on differences in total burned area, date of fire detection ("date of burn" (DOB)) and fire patch morphology. The aim is to obtain indications why the different burned area products differ and to discuss the implications for the Fire_cci Option 1 fuel consumption constrain analysis.

4.1. 2005 Black Tuesday Eyre Peninsula bushfire, SA, Australia

From January 2005, 10th afternoon to 12th, a single bushfire burned 772 km² on Eyre Peninsula, South Australia (Figure 13). It took further 9 days of activity by firefighters to extinguish smouldering logs and fence posts before the fire was finally declared out on 20 January². The fire, which claimed the lives of nine people and injured 115, is documented in detail Schapel (2008).

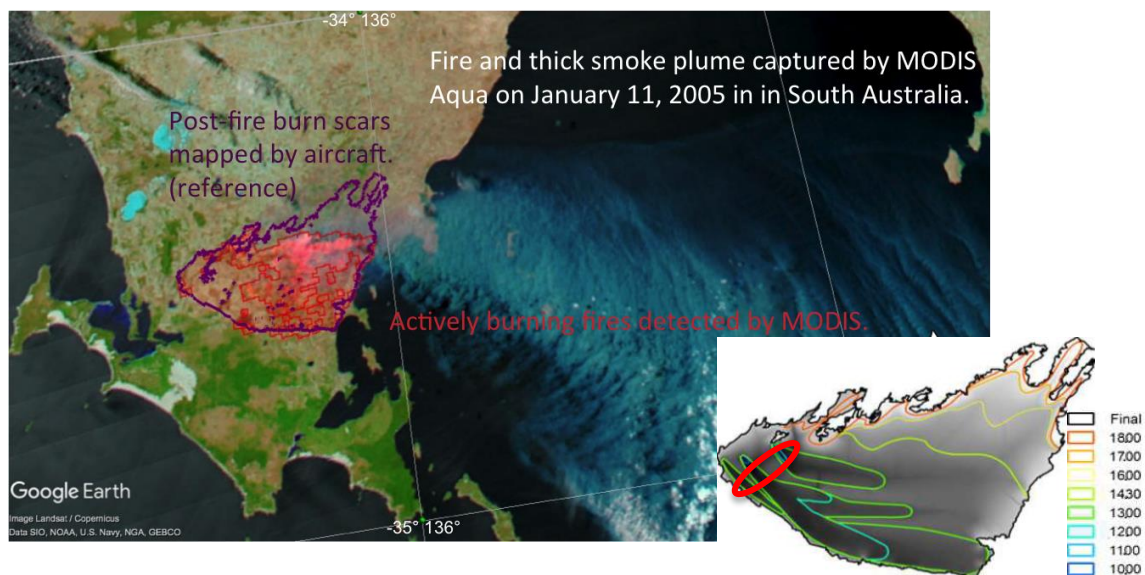


Figure 13: Google Earth Map of Eyre Peninsula, South Australia displaying an MODIS Aqua false-colour infrared image³ that shows huge fires and smoke plumes on January 11, 2005. Places where MODIS detected actively burning fire are outlined in red while areas of intense flaming appear in bright pink. The purple overlay displays the final perimeters of the burn scars as mapped by aircraft on January 17, 2005 (Data source: DEWNR⁴). The bottom right insert illustrates the

² <http://www.australianweathernews.com/news/2005/050111N.HTM>

³ https://eoimages.gsfc.nasa.gov/images/imagerecords/5000/5163/ge_05163.kml, last downloaded September 20, 2017.

⁴ Fire history spatial dataset provided by the Department of Environment, Water and Natural Resources (DEWNR), Government of South Australia (ISO19115/ISO19139 XML; <https://data.sa.gov.au/data/dataset/e5434c77-9815-48e6-8ea7-fb35c78f6786>), last downloaded July 12, 2017.



progression of the fire on January 11th, 2005 by hourly isochrones (Newnham et al. 2013). The red circle shows the approximate area burned on January 10th, 2005 (Johnston et al. 2010).

The fire started in the northwest of the fire perimeter shown in Figure 13. Approximately 20 km² was burned on 10th January (Johnston et al. 2006). The fire then rapidly progressed south and eastwards as a result of strong winds. By the evening of the 11th January, the fire had almost reached the final fire perimeter (Figure 13). The fire burned grassland, stubble, shrubby woodland and forest fuels, with the most predominant fuel being wheat stubble.

The comparison to the reference (REF) at the pixel level (Figure 14) indicates that Fire_cci 4.1 and MCD45 largely miss the westerly part of the final burn perimeter, and, in addition, depict a more patchy fire pattern (Figure 15). In contrast, MCD64C5 and MCD64C6 largely reproduce the actual fire perimeter. However, MCD64C6 and notably MCD64C5 exhibit several unburned island, which are much larger than in the REF burn perimeter. In addition, both products are unable to reproduce the area burned in the north-easterly "fingers" of the fire.

In terms of temporal mapping of the fire event, MCD64C5 and in particular MCD64C6 correctly assign most fire pixels to January 11th, 2005 (orange pixels DOB 11). The products also correctly reflect that the eastern parts of the final burn perimeter burned later than the western parts. A few scattered pixels in MCD64 products have DOB values of 13 to 16, hence after the actual fire. Interestingly, there are also few pixels with a DOB of 9, so clearly before the actual fire event started. In addition, there are fire pixels with DOB of 10, but not in the very north-western region where the fires were burning on January 10th. There is instead a cluster of pixels with DOB of 10 in the eastern outer perimeter of the fire. MCD64C5 also shows DOB values prior or after the actual fires, yet this feature is more pronounced than in MCD64C6. In MCD45, most fire pixels have a DOB value of 12, which is a one-day delay to the actual time of burning. Here again, there are several pixels with DOB values prior or after the actual fires. From the distribution of the DOB values, the temporal progression of the actual fire progression from the northwest to the west and east is not discernible.

As a complement, the mapping of the fire event in the recently released Fire_cci 5.0 pixel product is shown in Figure 16. The MODIS-based Fire_cci 5.0 product assigns most fire pixels to January 12th, 2005, i.e. to one day after most of the pixels actually burned. In the product, the actual fire event appears to consist of several individual fire patches, with unrealistically large unburned islands in the west and southeast of the actual fire perimeter shown in Figure 14.

The discrepancies between actual and satellite-derived DOB values cannot be explained by the geographical time difference. The Black Tuesday fire event started at around 3pm local time on January 10th, 2005, which corresponds to January 10th, 2005, 4:30am UTC.

Fire_cci 4.1 assigns most fire pixels to a DOB after the actual fire event (DOB 15: 23% of all pixels; DOB 24: 50%; DOB 43: 8%; DOB 53: 0.3%) and only 19% to a DOB during the actual fire event (DOB = 12) (Figure 17). In contrast to the MODIS products, no Fire_cci 4.1 pixel has a DOB prior to the actual fire event (Figure 15).

Since burn pixels with a strongly delayed detection do not have a lower confidence level (Figure 17 and Figure 18), the confidence level cannot be used to identify delayed detections. When discussing these results within the Fire_cci team, it was discovered that due to a misunderstanding, the confidence layer contained in the Fire_cci v4.1 product is directly taken from the MERIS processing, and is not the result of a logistic

regression model which was calibrated with reference data – as stated in the product's user guide (Pettinari et al. 2016).

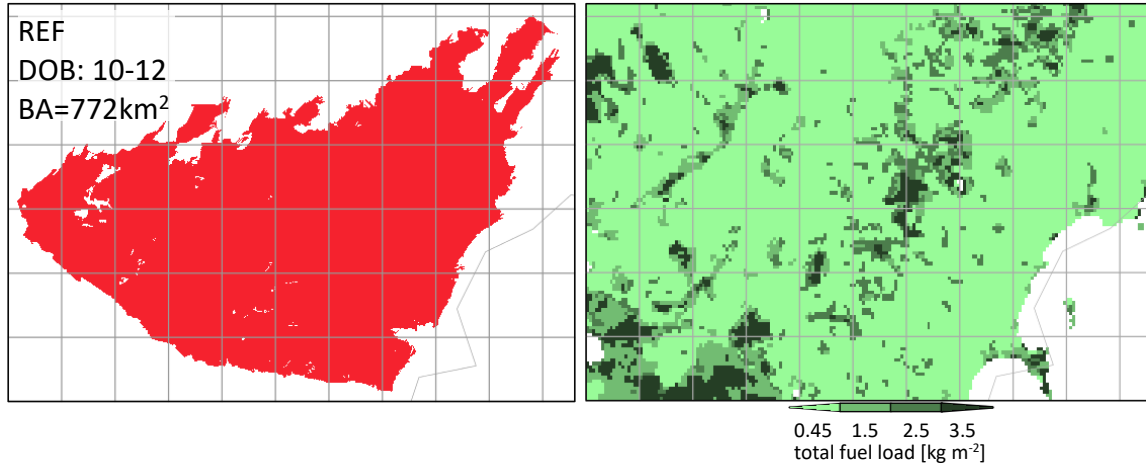


Figure 14: (a) Final perimeter of the burn scar as mapped by aircraft on January 17, 2005 (Data source: DEWNR(4)) for the domain of the Black Tuesday Eyre Peninsula bushfires (LON LAT box: 135.5,136.03,-34.65,-34.34). The actual fire event took place between Day of Burn (DOB) 10 to 12. Total area burned is given in the top left of the panel (left). (b) Map indicating the fuel load distribution. The map is derived by combining the fuel load estimates for different fuel categories by Newnham et al. (2013) with the LandCover_cci land cover map of the year 20045 (right).

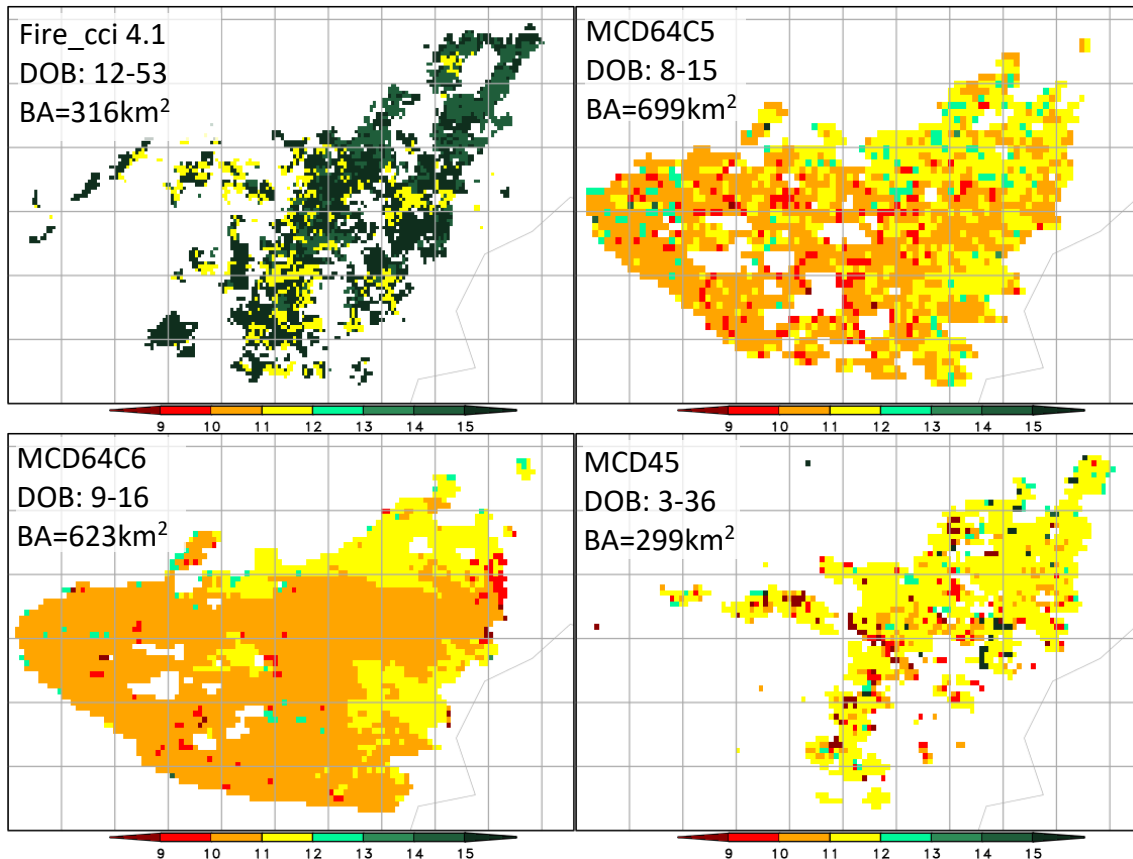


Figure 15: Day of burn (DOB) as given in pixel products for January to February 2005 for the domain of the Black Tuesday Eyre Peninsula bushfires. In the top left of each panel, the DOB range and the total area burned (BA) is given. The actual fire event took place between DOB 10 to 12.

⁵ The fuel load estimates are assigned to the following LandCover_cci LC codes: Forests (total fuel load of 3.5 kg m⁻²) = LC 50-80, 140; woodland (2.5 kg m⁻²) = LC 40, 100, 110; pasture, cropland, grassland (0.45 kg m⁻²) = all remaining LC codes.

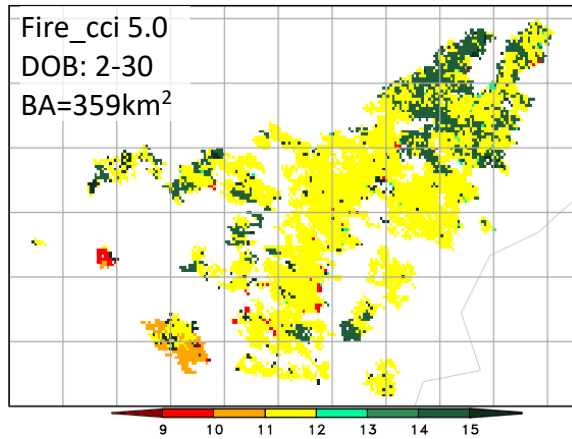


Figure 16: Day of burn (DOB) as given in the Fire_cci MODIS v5.0 pixel products for January to February 2005 for the domain of the Black Tuesday Eyre Peninsula bushfires.

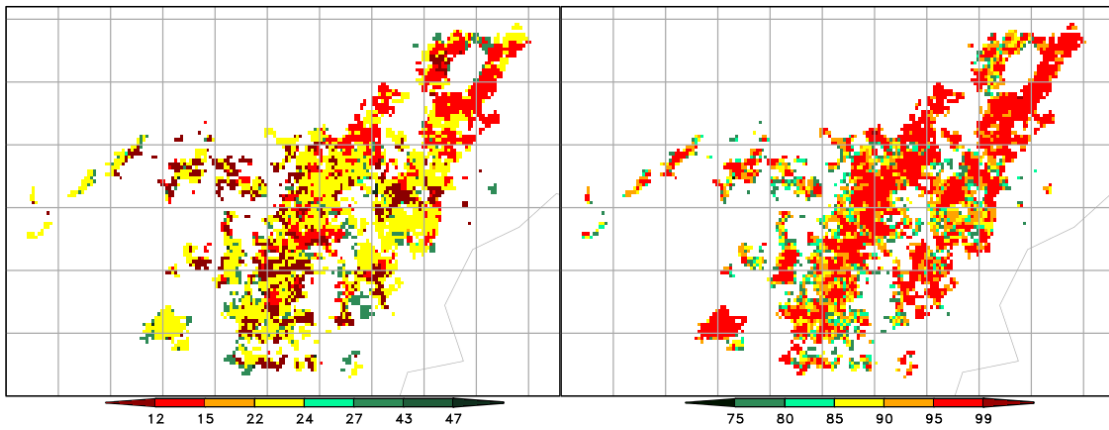


Figure 17: (a) Same as Figure 15 top left, but with different scaling (left). (b) Confidence level as given in the Fire_cci 4.1 pixel product for January and February 2005 (right).

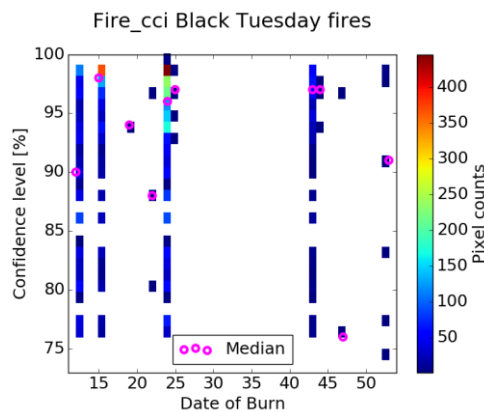


Figure 18: Density scatter plot relating Fire_cci 4.1 date of burn (DOB) and the corresponding confidence level for the domain of the Black Tuesday Eyre Peninsula bushfires across January and February 2005. The colour indicates the number density. In addition, the median confidence level per DOB is plotted.

Figure 19 compares 0.25 deg gridded monthly burned area and GFAS FRE data for January 2005 in the Eyre Peninsula domain. Compared to the field-surveyed reference (REF)⁴, all satellite products yield lower burned area estimates. MCD64C6 yields the smallest bias (10% lower). Fire_cci 4.1 maps only about half of the area that actually burned when comparing estimates for January 2005. MCD45 maps burned area in grid cells outside the REF perimeter, yet largely underestimate actual burned area. According to the official fire statistics (DEWNR), no other fire except the "Black Tuesday" occurred in January 2005 in this region. GFED4s increases MCD64C5 burned area by 1 to 6 km² per grid cell. Hence, the GFED4s approach not only supplements missing small fires but also "boosts" burned area of large fires.

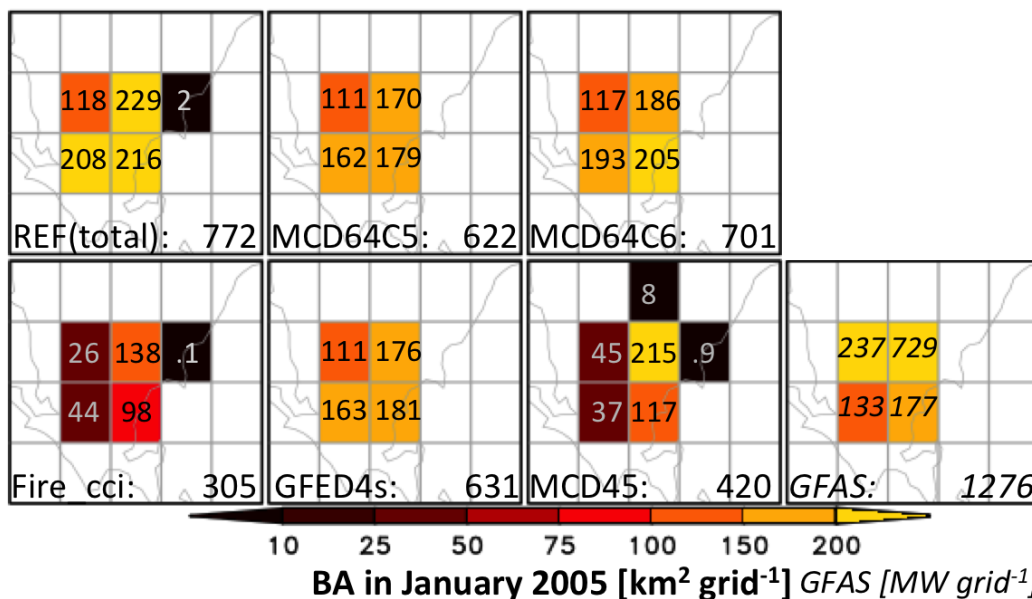


Figure 19: Burned area (BA) in South Australia in January 2005 as mapped by different inventories. REF denotes the aerial mapped burn scar reference as given by DEWNR⁽⁴⁾.

The strong temporal spacing of individual fire pixels in Fire_cci 4.1 has strong implications for the representation of the Black Tuesday Eyre Peninsula bushfire in the grid product: Figure 20 shows that in the biweekly Fire_cci 4.1 grid product, the bushfire appears to be burning across two months and appears to consist of many individual burn patches, while, in reality, it is a fire that burned for 3 days only.

The absolute value of the absolute bias in gridded burned area estimated by Fire_cci 4.1 (compared to the field-surveyed reference) is only slightly positively related to the value of the standard error (R^2 of 0.17 for linear correlation, $N=5$) and none of the 99% confidence intervals (CI) of the Fire_cci 4.1 burned area (BA) estimates (calculated from $CI_{99} = \text{Fire_cci BA} \pm 2.58 * \text{Fire_cci standard error}$) cover the reference burned area value (Figure 21a).

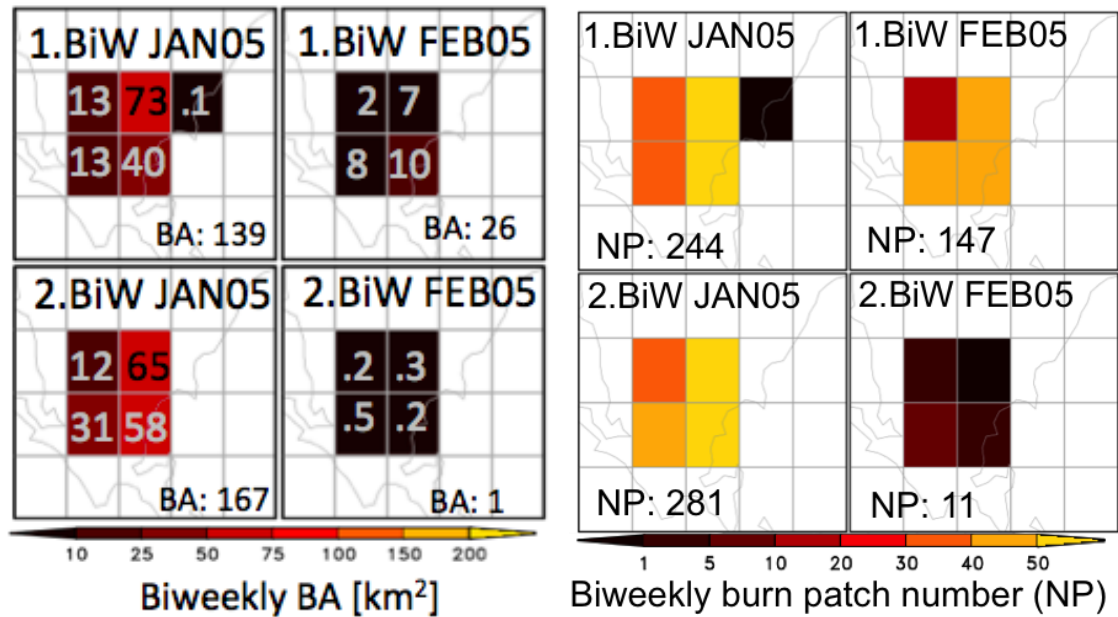


Figure 20: (a) Biweekly burned area (BA) (left) and (b) number of burn patches (NP) (right) in South Australia in January and February 2005 as mapped by Fire_cci 4.1.

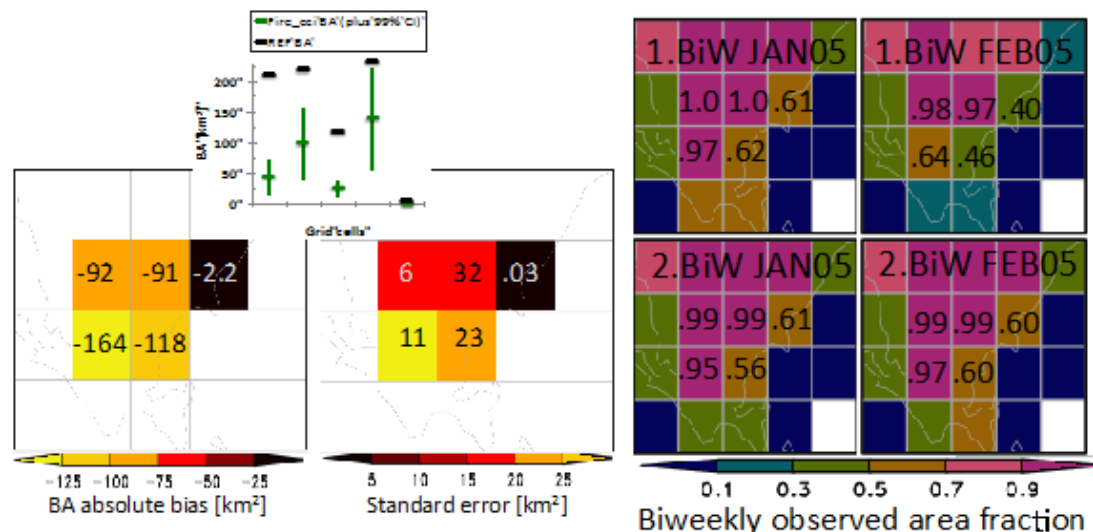


Figure 21: (a) Absolute burned area bias (Fire_cci 4.1 minus REF) and Fire_cci 4.1 standard error (SE) for the month January 2005. The SE is calculated from the biweekly standard errors by the root sum of the squares approach (Ratcliffe and Ratcliffe 2015). In the top insert, the 99% confidence intervals (CI) for the gridded Fire_cci burned area estimates for January 2005 and the corresponding reference BA values are shown (left). (b) Biweekly fraction of observed area in South Australia in January and February 2005 as mapped by Fire_cci (right).

Figure 21b illustrates that the Fire_cci 4.1 grid cells were well observed across January to February 2005, negating poor observational coverage as cause for the strong BA underestimation by Fire_cci.

MODIS burned area products, i.e. MCD64C5 (aka GFED4), MCD64C6 and GFED4s, do not provide a probabilistic confidence level estimate of the burn detection in their pixel products. Only the gridded GFED4 product contains a quantitative uncertainty estimate of the monthly burned area estimate. The latter relies on the validation effort of the MCD64C5 product described in Giglio et al. (2009, 2010), which was using a small number of Landsat scenes (50 scenes in total) in four very restricted geographical regions, namely Siberia, Western United States (plus northern Florida) and Southern

Africa. The analysis of the residuals that remain when regressing the burned areas of individual fire scars from MODIS with those from Landsat were used to conservatively estimate the net uncertainty in the 0.5 degree gridded, monthly MODIS BA estimates. They deduced five region(i)-specific BA uncertainty coefficients (CB) are used to calculate the "monthly burned area uncertainty" layer contained in the GFED4 product: $SD(i)=\sqrt{CB(i)*BA(i)}$, with SD being the "standard deviation" (Giglio et al. 2010) of the monthly BA estimate. As CB has been deduced for individual burn scars and not for total BA in a grid cell, the actual uncertainty in the grid cell is likely overestimated; potential error cancelling when multiple burn scars are present in the same grid cells is not accounted for. When interpreting SD as the standard deviation of the sample mean, the GFED4 "monthly burned area uncertainty" can be compared to the standard error (SE) estimate provided for the Fire_cci 4.1 gridded BA estimate (Figure 22 and Figure 21a). Compared to the Fire_cci 4.1 SE, the absolute GFED4 SE values tend to be higher while the relative SE values (i.e. SE relative to the BA estimate) are lower (on average 16% for GFED4 and 23% for Fire_cci 4/1). The 99% CI intervals of the GFED4 BA estimate cover the REF BA values with the exception of one grid cell where GFED4 BA estimate is zero.

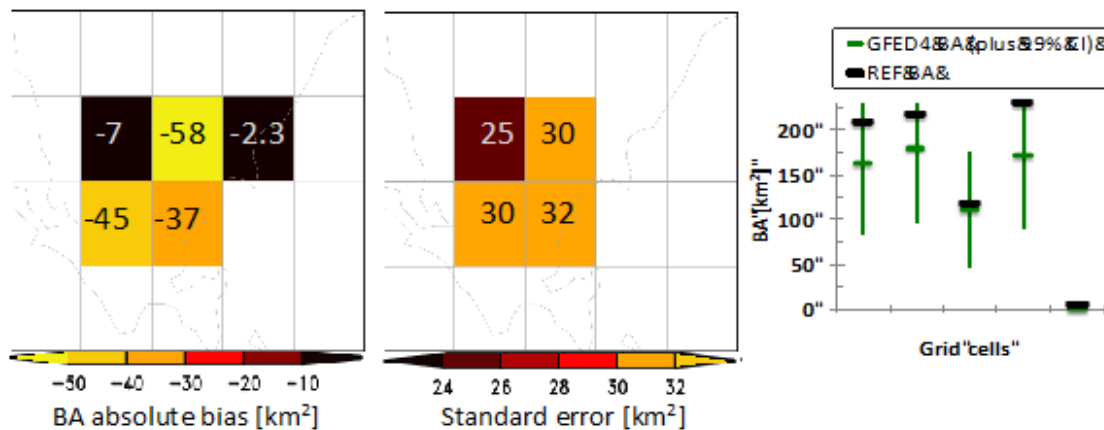


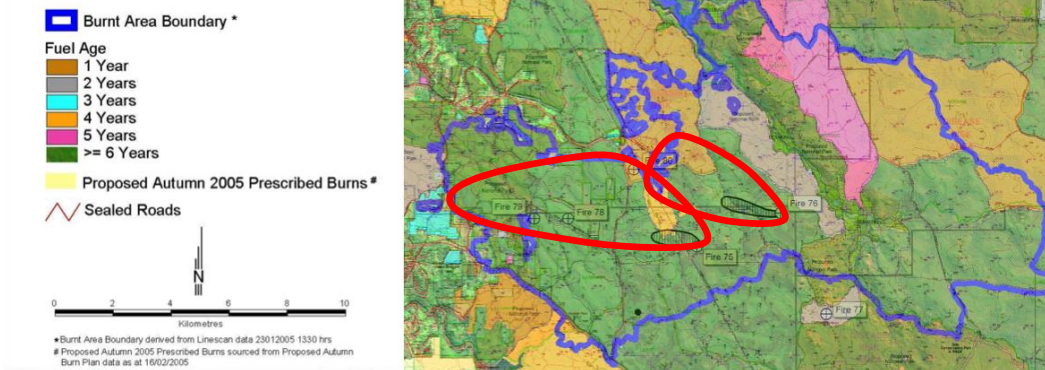
Figure 22: Same as Figure 21a, but for GFED4.

4.2. 2005 Pickering Brook bushfire, WA, Australia

The Pickering Brook wildfire burned 277 km² of Eucalyptus forest in the east of Perth, Western Australia, during the ten day period of 15-25 January 2005. The fire resulted from a number of deliberate ignitions, and subsequent spot fires identified as Perth Hills Fires numbers 71–80 (Cheney 2010). The first two fires started at 6pm local time on January 15th and progressed towards the northeast. Figure 23 shows the final reference (REF) burn scar of the fire as mapped by aerial survey. The fire burned in total 277 km², most of which in Eucalyptus forests.

Figure 24 shows the fire events as mapped by Fire_cci and the MODIS products MCD64C6, MCD64C5 and MCD45. With the exception of MCD45, all products closely reproduce the spatial pattern of the aerial surveyed burn perimeter and yield burned area estimates within ± 8% of REF. MCD45 underestimates BA by 43%.

Perth Hills Fire (15-28 January 2005) with Fuel Age and Proposed Autumn Burning



-- Perimeter DOB16

Figure 23: Burn scar (blue outline) of the Pickering Brook wildfire in January 2005 as mapped by aerial multispectral line scanning (Source: https://www.dpaw.wa.gov.au/images/documents/get-involved/n2n/schools/excursions/overlay_map1.jpg). The red lines schematically contour the perimeter of the area burned until January 16th, 10pm local time (Cheney 2010).

MCD64C5, and particularly MCD64C6, correctly map the general timing of the fire event, although in a few cases, fire pixels have assigned to a DOB before the fire event actually started (DOB of 13 and 14) and before the fire event could have been observed in daytime MODIS reflectance imagery. The first daytime MODIS observation from which burned area can be possibly mapped is from the 10am local time Terra overpass on February 16th, since the fire event started on the day before at 6pm local time and there are only night-time MODIS overpasses in between. Fire-related changes in daily MODIS surface reflectance observations can hence only be detected starting from February 16th. It is therefore unclear why some MCD64 pixels have an earlier date of burn. Also the MCD45 shows a pronounced premature detection of the Pickering Brook fire event. In this product, there is cluster of fire pixels with DOB of 14 in exactly the same area where the fire event initially started (Figure 23).

In terms of DOB, the Fire_cci 4.1 product exhibits a delayed detection of the actual fire event by around 7 to 22 days. 96% of all fire pixels fall either into DoB of 22 or 25 and 4% of all Fire_cci 4.1 burn pixels have a DoB of 34 (corresponding to February 2005, 3rd). In addition, there are 3 pixels with DOB between 41 and 47. Several of these "late-coming" out-of-the-fire-event burn pixels occur at the edges of the January burn scars. While the February fires add only 9.5 km² to the 254 km² of BA mapped by Fire_cci in January 2005, they strongly increase the total number of burn patches (20 in January compared to 93 in February 2005) (Figure 26). The delayed detection cannot be related to poor observational coverage since grid cells area fully observed, when consulting the fraction of observed area layer of the biweekly Fire_cci grid product: FOA is 1 in the bottom right grid cell all, and between .989 and .998 in the other grid cells shown in Figure 26 in the first three biweekly time steps of the year 2005. Figure 25 demonstrates that the pixels with a delayed detection cannot be unambiguously identified from the confidence level information.

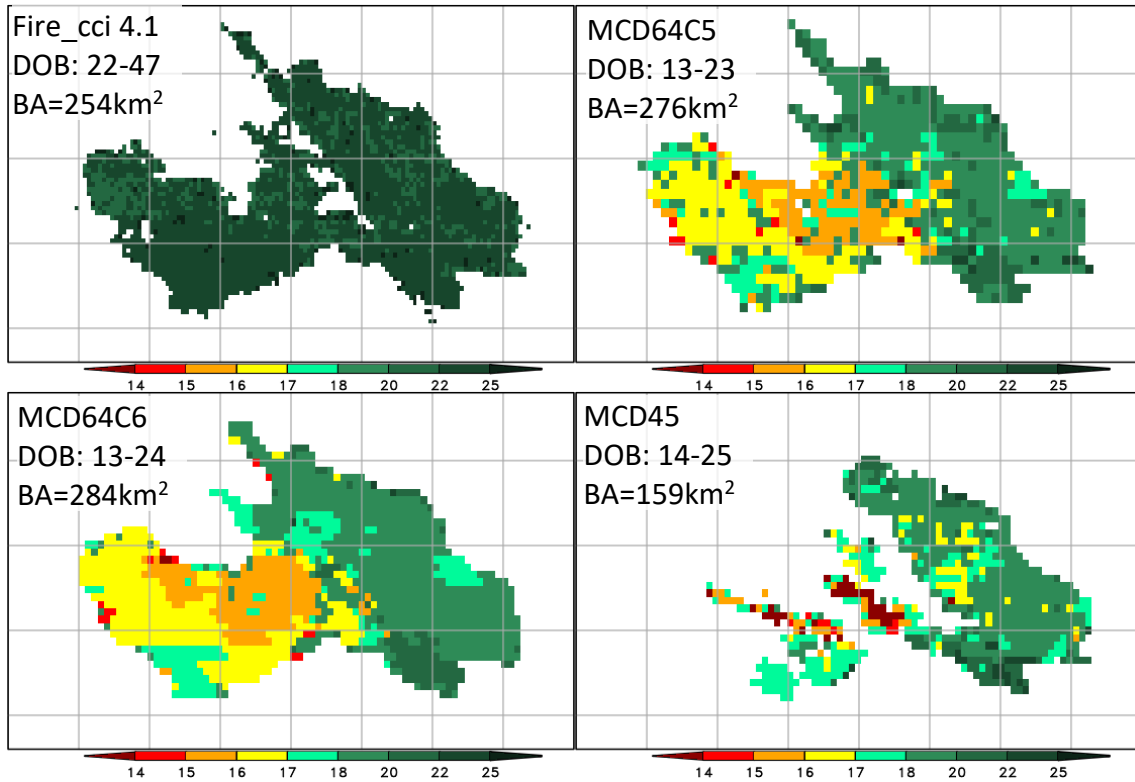


Figure 24: Day of burn (DOB) as given in pixel products for January to February 2005 for the domain of the Pickering Brook bushfire (LON LAT box: 116.05,116.45,-32.17,-31.96, grid lines with 0.05 degree spacing). In the top left of each panel, the DOB range is and the total area burned is given. The actual fire event took place between DOB 15 to 25. In the MODIS products, there is a separate around 4 km² burn patch at 31.15 deg South and 116.1 deg East with DOB between 43 to 52 which is masked out here.

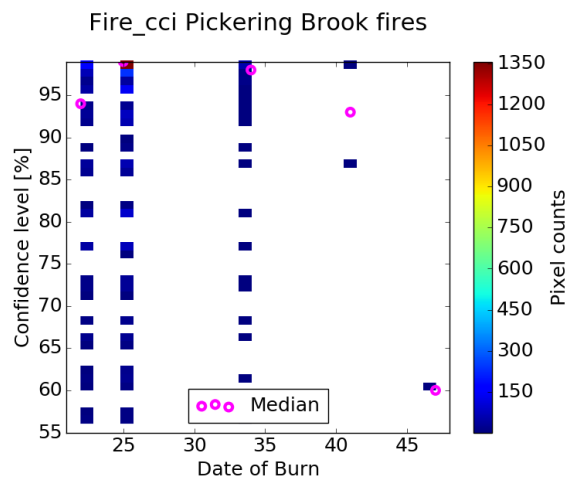


Figure 25: Density scatter plot relating Fire_cci 4.1 date of burn (DOB) and the corresponding confidence level for the domain of the Pickering Brook wildfire across January and February 2005. The colour indicates the number density. In addition, the median confidence level per DOB is plotted.



BA per grid in JAN05 (+ BA in FEB 05)

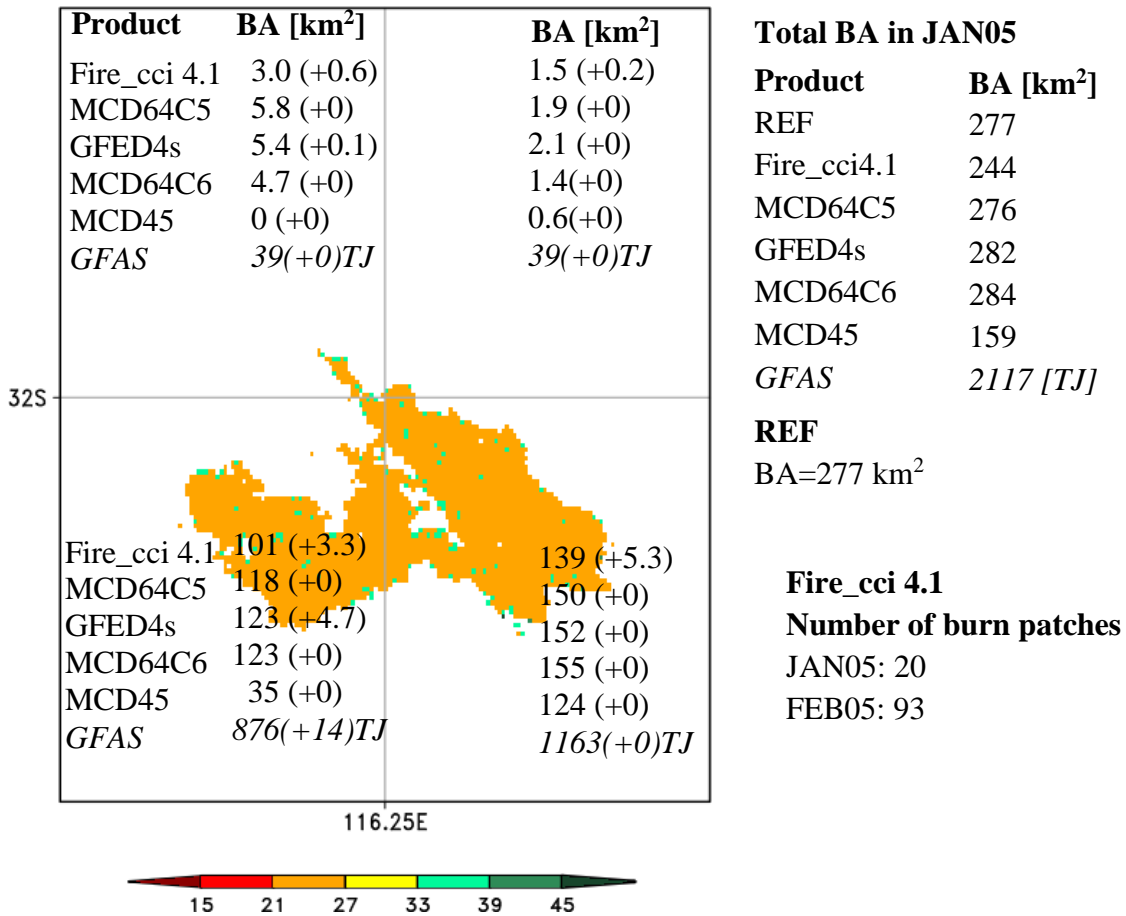



Figure 26: Burned area and FRR estimated for January and February 2005 for the Pickering Brook wildfire. Estimates are given for individual 0.25 grid cells and as summary statistics for the entire domain.

	Fire_cci Option 1 WP110 Basic consistency of fire observation report	Ref.:	Fire_cci_O1.D1_v1.0.docx		
		Issue	1.0	Date	23/01/2018
				Page	32

5. Conclusions and Recommendations for WP130

- A data repository comprising global 0.25 degree spatially gridded maps and time series of burned area (BA), fuel consumption and fuel characteristics has been established. The repository provides the data required for further analysis to be carried out in WP130 of Option 1.
- Spurious signals in the fire satellite products (e.g. false alarms due to volcanoes, highly reflective surfaces) can, in some case, drastically influence regional budgets. It is therefore recommended to rigorously cleanse all input datasets from potential false alarms by e.g. masking all grid cells with volcanic activity and areas with a high proportion of human infrastructure (urban or industrial agglomerations, airports, highways, gas flaring sites).
- The observational coverage of the burned area observations may strongly influence calculated fuel constraints and should therefore be taken into account in the Option 1 WP130 analysis.
- No robust information on the uncertainty of the burned area products in the Option 1 repository can be provided. As a consequence, there is currently no possibility to stratify the fuel consumption constrain analysis by the uncertainty of the burned area estimates.
- Errors in correctly assigning the day of burn may lead to strong artefacts in any analysis aiming at combining different burned area datasets with fire radiative power (FRP)-derived estimates in spatiotemporally explicit manner. It should be explored to what extent a temporal aggregation (e.g. combining only fire year integrated estimates of BA with corresponding estimates of FRP and fuel consumption, only) is a means to improve inter-product consistency.
- The Fire_cci Option 1 data repository still misses 0.25 degree gridded GFAS products. Instead of aggregating it with considerable interpolation errors from the operational 0.1 degree version of GFAS in CAMS, it has been decided to use the 0.05 degree version that is currently being produced by the German GFAS-CLIM project.



6. References

- Alonso-Canas, I., Chuvieco, E. 2015. Global burned area mapping from ENVISAT-MERIS and MODIS active fire data. *Remote Sensing of Environment* **163**, 140–152.
- Bai, Y., Feng, M., Jiang, H., Wang, J., Zhu, Y., Liu, Y. 2014. Assessing Consistency of Five Global Land Cover Data Sets in China. *Remote Sens.* **6**, 8739-8759. doi:10.3390/rs6098739.
- Cheney, N.P. 2010. Fire behaviour during the Pickering Brook wildfire, January 2005 (Perth Hills. Fires 71-80). *Conservation Science W. Aust.* **7**, 451-468.
- Giglio, L., Loboda, T., Roy, D.P., Quayle, B., Justice, C.O. 2009. An active-fire based burned area mapping algorithm for the MODIS sensor. *Remote Sensing of Environment* **113**, 408–420.
- Giglio, L., Randerson, J. T., van der Werf, G. R., Kasibhatla, P. S., Collatz, G. J., Morton, D. C., and DeFries, R. S. 2010. Assessing variability and long-term trends in burned area by merging multiple satellite fire products. *Biogeosciences*, **7**, 1171-1186, <https://doi.org/10.5194/bg-7-1171-2010>.
- Giglio, L., Randerson, J., Werf, G. 2013. Analysis of daily, monthly, and annual burned area using the fourth-generation global fire emissions database (GFED4). *J Geophys Res Biogeosciences* **118**, 317–328.
- Johnston, P., Milne, G., Kelso, J. 2006. A heat transfer simulation model for wildfire spread. *Forest Ecology and Management* **234**, S78, doi:10.1016/j.foreco.2006.08.114.
- Kaiser, J. W., Heil, A., Andreae, M. O., Benedetti, A., Chubarova, N., Jones, L., Morcrette, J.-J., Razinger, M., Schultz, M. G., Suttie, M., and van der Werf, G. R. 2012. Biomass burning emissions estimated with a global fire assimilation system based on observed fire radiative power. *Biogeosciences*, **9**, 527-554, <https://doi.org/10.5194/bg-9-527-2012>.
- Newnham, G., Blanchi, R., Siggins, A., Opie, K., Leonard, J. 2013. Bushfire Decision Support Toolbox Radiant Heat Flux Modelling: Case Study Two, Wangary, South Australia. Report to the Bushfire Cooperative Research Centre. Australia. Available online at http://bushfirecrc.com/sites/default/files/managed/resource/case_study_two_-_wangary_south_australia.pdf.
- Pettinari, M. L. and Chuvieco, E. 2016. Generation of a global fuel data set using the Fuel Characteristic Classification System. *Biogeosciences*, **13**, 2061-2076, <https://doi.org/10.5194/bg-13-2061-2016>.
- Pettinari, M.L., Chuvieco, E., Alonso-Canas, I., Storm, T., Padilla Parellada, M. 2016. ESA CCI ECV Fire Disturbance: Product User Guide, version 2.1. Available at:<http://www.esa-fire-cci.org/documents>
- Randerson, J., Chen, Y., Werf, G., Rogers, B., Morton, D. 2012. Global burned area and biomass burning emissions from small fires. *Journal of Geophysical Research: Biogeosciences* **117**, G04012, doi:10.1029/2012JG002128.
- Roy, D.P., Boschetti, L., Justice, C.O., Ju, J. 2008. The collection 5 MODIS burned area product—Global evaluation by comparison with the MODIS active fire product. *Remote Sensing of Environment* **112**(9), 3690-3707.
- Schapel, A.E., 2008. Inquest into the deaths of Star Ellen Borlase, Jack Morley Borlase, Helen Kald Castle, Judith Maud Griffith, Jody Maria Kay, Graham Joseph Russell, Zoe Russell-Kay, Trent Alan Murnane and Neil George Richardson. Coroners Court, Government of South Australia, Adelaide, Australia, 703pp. Available online at <http://www.courts.sa.gov.au/CoronersFindings/Lists/Coroners%20Findings/Attachments/310/Wangary%20Fires%20Inquest%20-%20MODIFIED%20and%20FINAL%20February%202008.pdf>.
- van der Werf, G. 2017. D_O1.2 Internal report on uncertainties of CC and AFL, for use in WP130 of Fire CCI project. August 2017.
- van der Werf, G. R., Randerson, J. T., Giglio, L., van Leeuwen, T. T., Chen, Y., Rogers, B. M., Mu, M., van Marle, M. J. E., Morton, D. C., Collatz, G. J., Yokelson, R. J., and Kasibhatla, P. S. 2017. Global fire emissions estimates during 1997–2016. *Earth Syst. Sci. Data*, **9**, 697-720, <https://doi.org/10.5194/essd-9-697-2017>.